AD_____

Award Number: W81XWH-11-1-0332

TITLE: High-Resolution Large-Field-of-View Ultrasound Breast Imager

PRINCIPAL INVESTIGATOR: Patrick LaRiviere

CONTRACTING ORGANIZATION: University of Chicago
Chicago, Illinois 60637-5418

REPORT DATE: June 2012

TYPE OF REPORT: Annual

PREPARED FOR: U.S. Army Medical Research and Materiel Command
Fort Detrick, Maryland 21702-5012

REPORT DOCUMENTATION PAGE

Form Approved
OMB No. 0704-0188

1. REPORT DATE	2. REPORT TYPE	3. DATES COVERED
01-06-2012	Annual	1 JUN 2011 - 31 MAY 2012

4. TITLE AND SUBTITLE

High Resolution Large Field of View Ultrasound Breast Imager

5a. CONTRACT NUMBER

5b. GRANT NUMBER
W81XWH-11-1-0332

5c. PROGRAM ELEMENT NUMBER

6. AUTHOR(S)
Patrick J. La Riviere

E-Mail: pjlarivi@uchicago.edu

5d. PROJECT NUMBER

5e. TASK NUMBER

5f. WORK UNIT NUMBER

7. PERFORMING ORGANIZATION NAME(S) AND ADDRESS(ES)

University of Chicago

Chicago, Illinois 60637-5418

8. PERFORMING ORGANIZATION REPORT NUMBER

9. SPONSORING / MONITORING AGENCY NAME(S) AND ADDRESS(ES)
U.S. Army Medical Research and Materiel Command
Fort Detrick, Maryland 21702-5012

10. SPONSOR/MONITOR'S ACRONYM(S)

11. SPONSOR/MONITOR'S REPORT NUMBER(S)

12. DISTRIBUTION / AVAILABILITY STATEMENT
Approved for Public Release; Distribution Unlimited

13. SUPPLEMENTARY NOTES

14. ABSTRACT
In this work, we are seeking to construct and test the first practical full-field transmission ultrasound breast imaging system. The system will have a large field-of-view capable of producing 2D images of the entire breast in near real-time. Because it uses a fixed imaging geometry that does not involve scanning, it will also circumvent the operator-dependence of conventional ultrasound imaging methods. We have made substantial progress in this first year of the project. Most tasks in the original Statement of Work for year 1 have been completed on schedule. The only delay has been in the optimization, fabrication, and acceptance testing of the lenses, which we had scheduled to complete within 9 months and is just now wrapping up in the 13th month. This arose mainly from the need to alter our original design from a refraction-based system to a reflection-based system, due to unacceptably high levels of acoustic attenuation predicted in the refraction-based system.

15. SUBJECT TERMS: Breast imaging, acoustomammography, breast cancer

16. SECURITY CLASSIFICATION OF:			17. LIMITATION OF ABSTRACT	18. NUMBER OF PAGES	19a. NAME OF RESPONSIBLE PERSON
a. REPORT	b. ABSTRACT	c. THIS PAGE			USAMRMC
U	U	U	UU	47	19b. TELEPHONE NUMBER *(include area code)*

Table of Contents

Page

Annual Report for W81XWH-11-1-0332
PI: Patrick La Riviere

INTRODUCTION:

In this work, we are seeking to construct and test the first practical full-field transmission ultrasound breast imaging system. The system will have a large field-of-view capable of producing 2D images of the entire breast in near real-time. Because it uses a fixed imaging geometry that does not involve scanning, it will also circumvent the operator-dependence of conventional ultrasound imaging methods. The compact vertical design mimics the form factor of mammography systems and would provide a basis for later incorporation of an x-ray source and detector, which would allow for routine dual-modality x-ray and acoustic imaging for screening and diagnosis. If successful, this work will provide the basis for a dual-modality ultrasound and mammography imaging system that could help improve early detection of breast cancer, especially in young women with dense breasts, which are often not well visualized mammographically. It would also help reduce false positives, which add to the expense and anxiety associated with current approaches to breast cancer screening.

BODY:

Summary: We have made substantial progress in this first year of the project. Most tasks in the original Statement of Work for year 1 have been completed on schedule. The only delay has been in the optimization, fabrication, and acceptance testing of the lenses, which we had scheduled to complete within 9 months and is just now wrapping up in the 13th month. This arose mainly from the need to alter our original design from a refraction-based system to a reflection-based system, due to unacceptably high levels of acoustic attenuation predicted in the refraction-based system.

Aim 1: To design and construct a high-resolution, large field of view ultrasound breast imager by combining a super high-resolution AO sensor and a large aperture acoustic lens.

Task 1: Design, fabricate, and test sound source

1.a. Simulate acoustic propagation from array of 9 2.7" elements to confirm suitability of design choice (U of C; mos. 1-2).

We have developed theory and software necessary to simulate the acoustic field emanating from square transducer elements. In brief, we made use of standard Rayleigh-Summerfield diffraction theory and the angular spectrum decomposition to develop expressions for the field propagating from a rectangular piston-like transducer. By the linearity of the resulting equations, we can use superposition to determine the field produced by an array of square or rectangular transducers.

The details are provided in Appendix A, but the key results are shown in Fig 1 below, which illustrates the normalized in-plane acoustic intensity distribution at a distance 2 inches from a 3" by 3" square transducer piston operating at a CW frequency of 3.35 MHz. The figure shows both a surface plot and a color mapped intensity distribution.

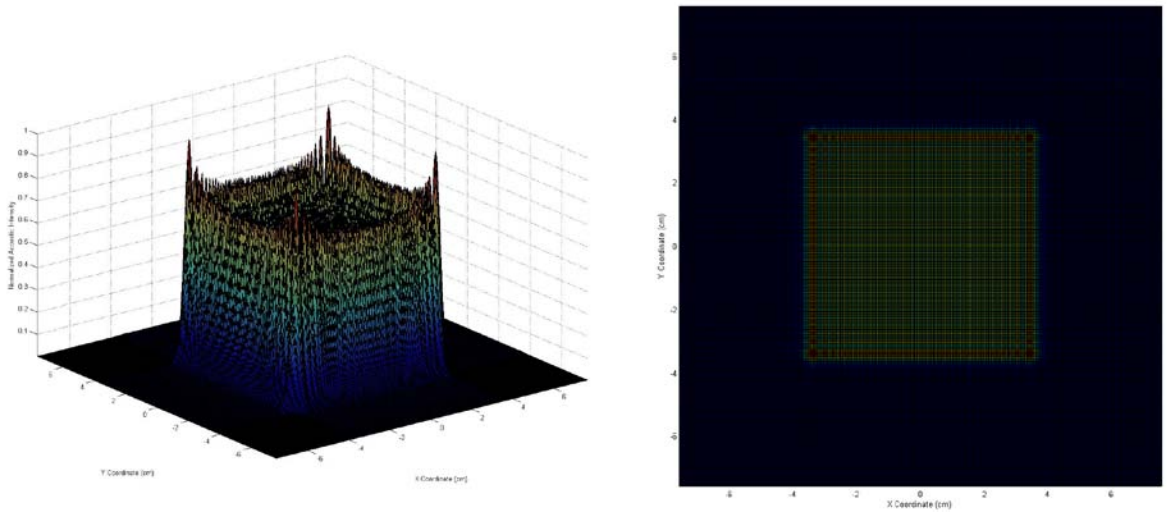

Figure 1: (Left) The normalized in-plane acoustic intensity distribution for a 3" by 3" square transducer piston operating at a CW frequency of 3.35 MHz. The pressure field intensity is depicted in the plane parallel to the transducer surface at a distance of 2", and a background medium of water has been assumed. We note that the square modulus of the acoustic pressure field is plotted. (Right) This figure presents the same information as the left plot but shows the spatial distribution of acoustic intensity looking at the plane of interest head-on. For a planar detector positioned 2" from the transducer surface, one would expect to observe this type of diffraction pattern for an image acquired with no scattering object present.

1.b. Fabricate source array (Santec; mos. 2-3)

A large-area sound source has been designed and fabricated with four 4 MHz, 3"x3" size elements. The original plan called for working at 3.35 MHz, but technical difficulties necessitated a change to 4 MHz, which should not affect any of the properties of the planned system. A quarter-wavelength acoustic matching layer was provided to allow efficient operation in water. Each element was electrically tuned to match to the 50-Ohm impedance of an RF Amplifier powered by a 4.0 MHz electrical signal from a digital function generator. An RF power splitter was also designed and built to distribute RF power equally to all 4 elements of the sound source. First-level software was also developed to allow digital control of acoustic power output of the sound source. The current design is being extended to build a larger source to cover the 8"x8" field area.

1.c Test source and compare with simulation results (U of C; mos. 3-4)

Our preliminary comparisons indicate good agreement between the real and simulated fields. More detailed comparison work is ongoing.

Task 2: Fabricate and test AO sensor

2.a Fabricate 1" X 1" AO sensor (Santec; mos. 4-5)

At least three 4 MHz AO sensors have been built. We were able to overcome some technical challenges and build even larger sensors than originally planned. The detection area of each sensor was at least 2"x2". The acoustic detection sensitivity of these sensors was found to be in the milliWatt/cm^2 range.

The angular acceptance of the AO sensor is at least 20^o about normal incidence condition. The acoustic detection sensitivity was quite dependent on the acoustic beam angle, and might impact image quality. However, this needs to be studied using the acoustic lens (or mirrors) being designed so that if needed, the AO sensor design can be change to minimize the angular effect. The milliWatt/cm^2 range acoustic detection sensitivity of the AO sensor should be adequate to allow us to operate the Breast Imager below the FDA specified safety standard.

2.b Test resolution and sensitivity of AO sensor (U of C; mos. 5-6)

We sought to characterize the spatial resolution of the prototype transmission ultrasound imaging system by deriving estimates for the edge spread function (ESF), the line spread function (LSF), and the pre-sampled modulation transfer function (MTF) of the system. We also sought to characterize the noise properties of the prototype transmission ultrasound imaging system by determining an estimate for the noise power spectrum (NPS) of the system.

Spatial Resolution Analysis

The spatial resolution analysis was performed using the angled edge technique originally proposed by Reichenbach *et al*. [1], in which use of a small (~ 3^o) edge angle permits finer sampling of the system ESF than the pixel pitch of a digital detector, thus minimizing the possibility of MTF aliasing. A transmission ultrasound image of a slightly angled knife edge was acquired with temporal averaging to reduce noise. A segment of the knife edge image is shown in Figure 2. Each row of pixels in Figure 2 provided a shifted sample of the knife edge. The individual rows were spatially registered by estimating the edge position within

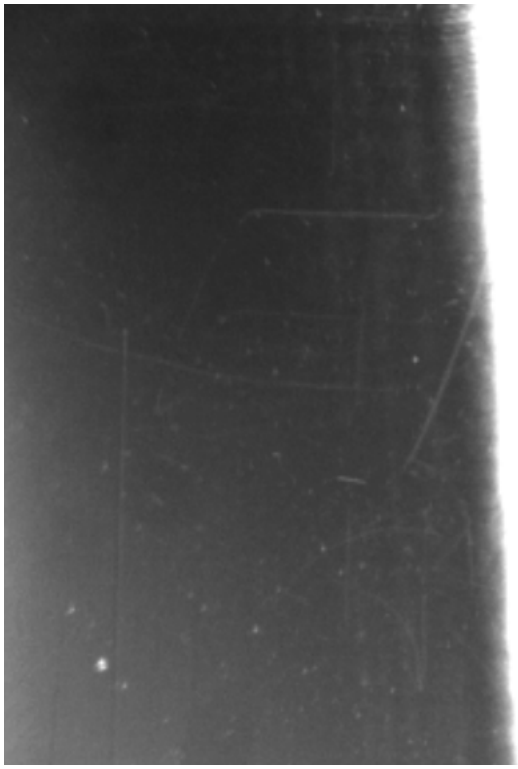

Figure 2: Image of the knife edge used to compute the pre-sampled MTF of the imaging system. The image was acquired using a peak transducer voltage of 0.7 V. Continuous frequency sweeping of 3.25-3.45 MHz at 100 MHz/s was also employed to minimize speckle artifacts due to acoustic wave coherence.

After shifting each row of pixel values by the estimated edge location, the spatially registered data points were averaged over .0625-mm intervals to obtain an estimate of the system ESF. Following the work of Boone and Seibert [2], the measured ESF data was fit to a combined error function and exponential fit of the form

$$\mathrm{ESF}(x) = \mathbf{a}\,\mathrm{sgn}(x - x_0)\left\{1 - \exp\left(-\mathbf{b}|x - x_0|\right)\right\} + \mathbf{c}\left\{\mathrm{erf}\left(\sqrt{\mathbf{d}}(x - x_0)\right)\right\} + \mathbf{e}.$$

Analytic estimates for the normalized system LSF and MTF were determined from the fit parameters ***a****,* ***b****,* ***c****,* ***d****,* ***e****, and* x_0 *according to the relations*

$$\mathrm{LSF}(x) = \frac{1}{2(\mathbf{a}+\mathbf{c})}\left[\mathbf{ab}\exp\left(-\mathbf{b}|x - x_0|\right) + 2\mathbf{c}\sqrt{\frac{\mathbf{d}}{\pi}}\exp\left(-\mathbf{d}(x - x_0)^2\right)\right].$$

$$\mathrm{MTF}(f) = \frac{1}{\mathbf{a}+\mathbf{c}}\left[\mathbf{c}\exp\left(-\frac{\pi^2 f^2}{\mathbf{d}}\right) + \mathbf{a}\left(1 + \frac{4\pi^2 f^2}{\mathbf{b}^2}\right)^{-1}\right].$$

Spatial Resolution Analysis Results

Figure 3 presents the measured ESF data points with overlaid exponential-error function regression model. The statistics of the computed fit are also provided.

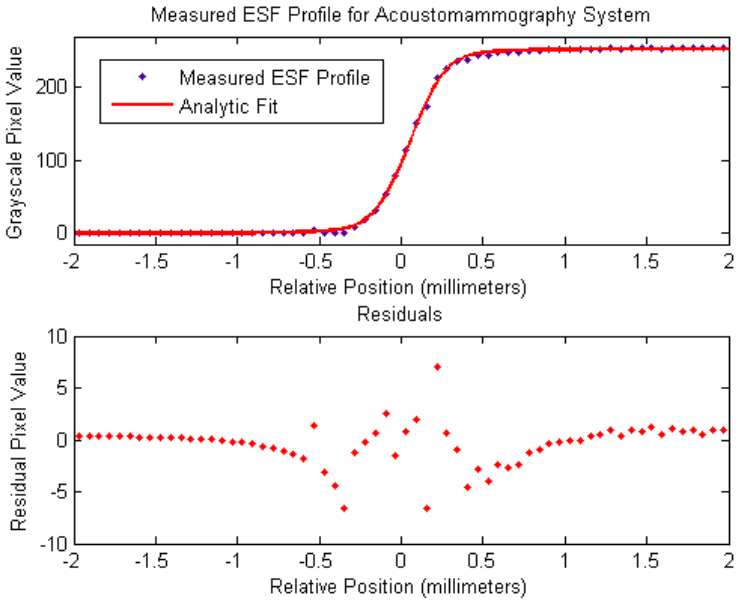

Regression Statistics

Fit Coefficients:

a = 17.77

b = 3.22 mm^{-1}

c = 108.9

d = 17.4975 mm^{-2}

e = 126.3

x_0 = 0.05298 mm

Goodness of fit:

r^2 = 0.9999

RMSE: 1.426

Figure 3: Measured ESF data and analytic regression model with residual subplot. The r^2 value for the regression curve is 0.9999, and the root-mean-square error (RMSE) is only 1.15% of the mean measured ESF value. These statistics indicate that the combined exponential-error function regression model provides an excellent fit to the measured data.

Figure 4 shows the normalized analytic LSF and the analytic pre-sampled MTF derived from the regression equation used to fit the ESF data in Figure 6.

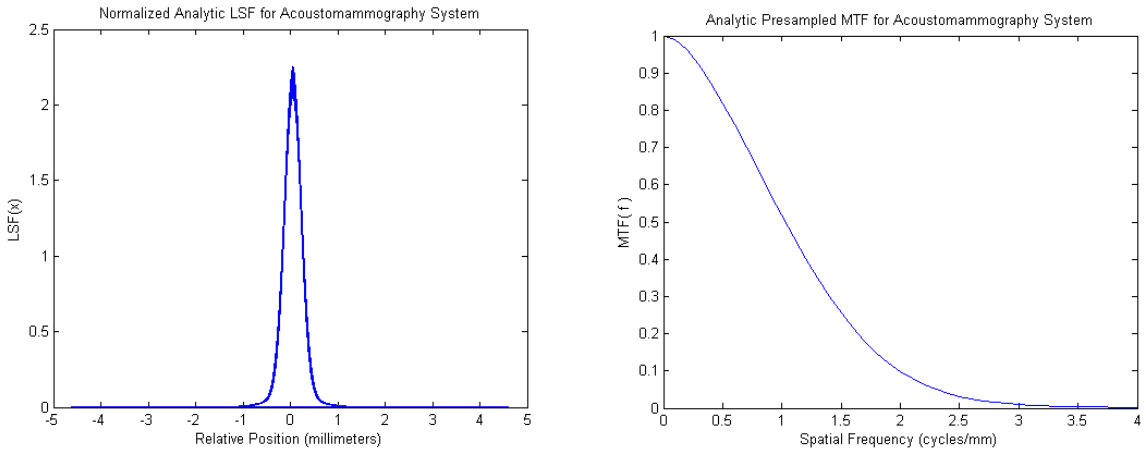

Figure 4: The normalized analytic LSF and the analytic pre-sampled MTF for the transmission ultrasound imaging system. These curves were obtained from the fitting parameters of the combined exponential-error function regression model used to fit the measured ESF data. The full-width-at-half-maximum (FWHM) of the system LSF indicates an approximate spatial resolution of 400 microns.

The FWHM of the analytic LSF was calculated to be 0.3997 millimeters, indicating an approximate spatial resolution of 400 microns for the prototype transmission ultrasound imaging system. The analytic curve for the pre-sampled MTF shows a typical Gaussian form. The curve is equal to unity at zero spatial frequency and falls off smoothly to nearly zero at the system Nyquist frequency (3.79 cycles/mm).

Noise Analysis

The NPS of the imaging system was determined by acquiring 25 detector flood images using the same transducer settings for each acquisition. One such image is included in Figure 5. For each flood image, a subsection of the total image matrix was extracted over which the detector illumination appeared highly uniform. The NPS of each subsection was computed by subtracting the mean pixel value <PV> and computing the square modulus of the two-dimensional discrete Fourier transform of the resulting matrix. In the continuum,

$$\mathrm{NPS}(\mathbf{f}) = \left| \int_{-\infty}^{\infty} \int_{-\infty}^{\infty} \left[\mathrm{PV}(\mathbf{r}) - \langle \mathrm{PV} \rangle \right] e^{-j2\pi \mathbf{f}\cdot\mathbf{r}} d^2\mathbf{r} \right|^2 .$$

The 25 separately computed noise power spectra were averaged to obtain a mean estimate for the NPS of the system. This estimate was normalized by its largest amplitude component and plotted as a two-dimensional function of spatial frequency **f**.

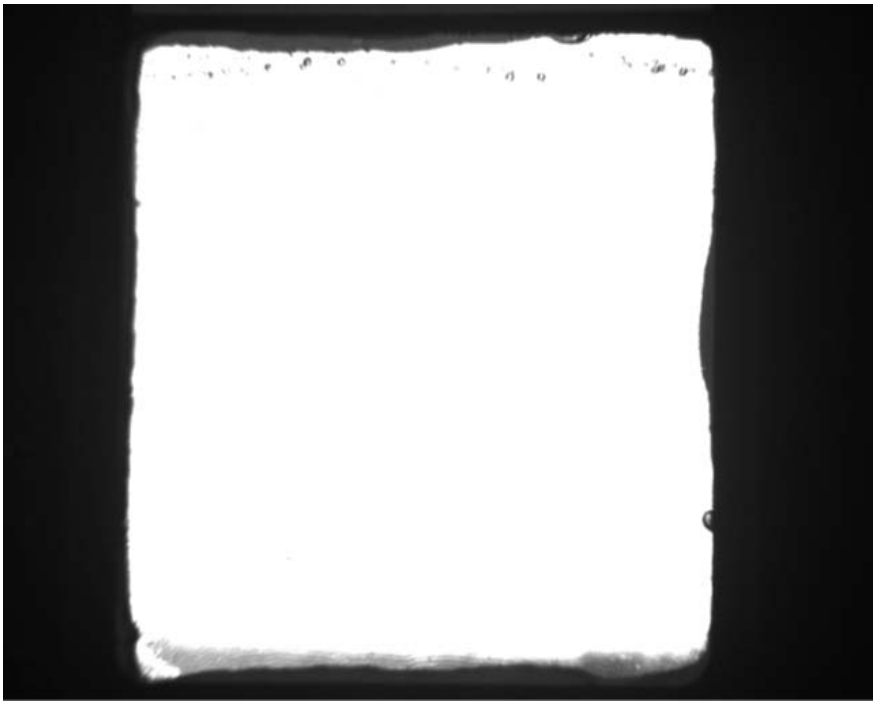

Figure 5: Example of one of the detector flood images used to estimate the NPS of the imaging system. The image shows highly uniform illumination of the AO detector field of view. A peak transducer voltage of 2.6 V and frequency sweeping of 3.25-3.45 MHz at a rate of 100 MHz/s were used because of the uniform detector illumination provided by these settings

Figure 6 presents an estimate of the two-dimensional NPS of the imaging system as a surface plot. The height of the NPS indicates the noise power contained per unit frequency bandwidth at each corresponding spatial frequency. It can be seen that significant noise power is contained at lower spatial frequencies near zero frequency. The NPS amplitude falls steadily when moving toward higher spatial frequencies.

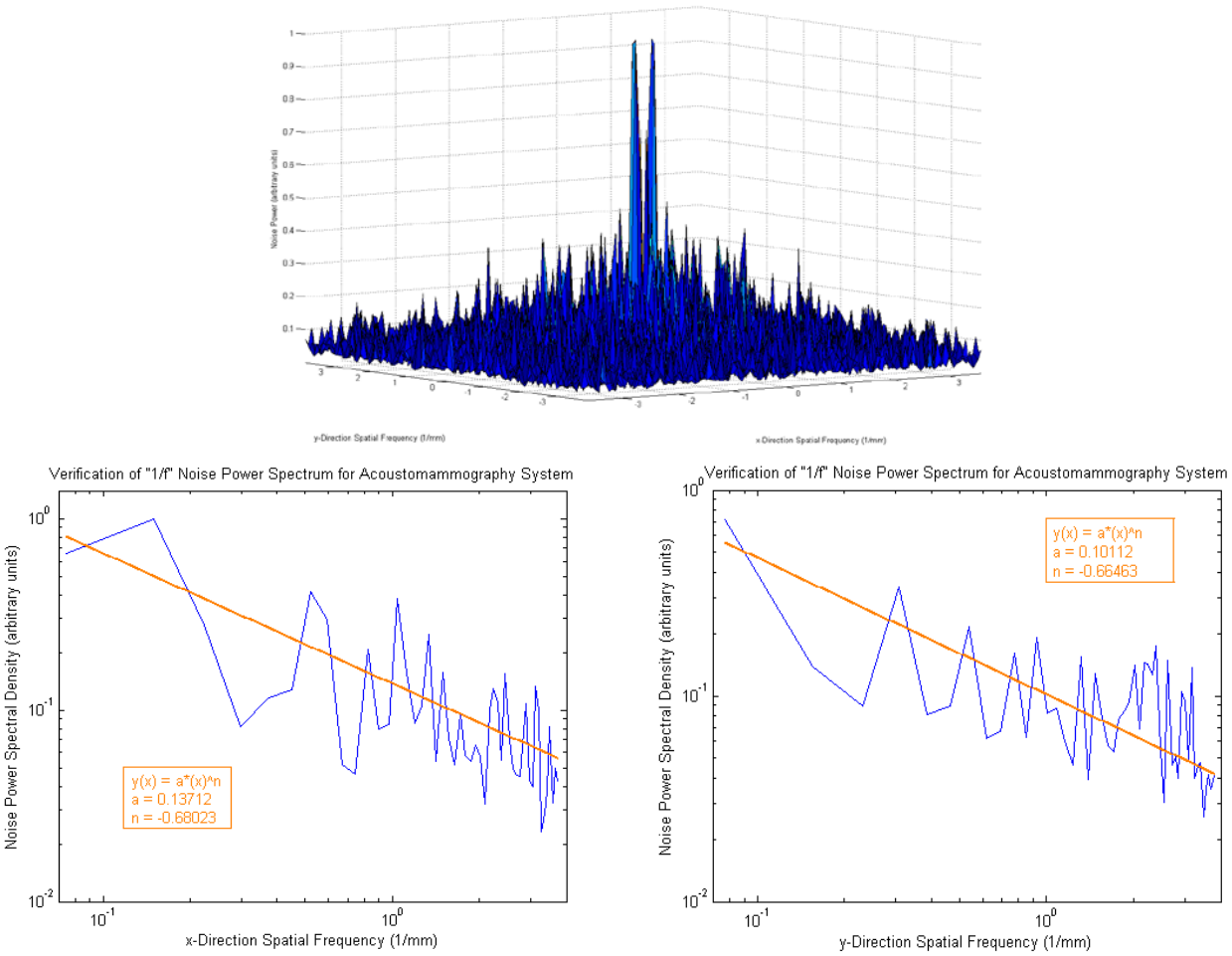

Figure 6: Surface plot of the two-dimensional NPS of the transmission ultrasound imaging system. The lower two graphs show single slices taken through the NPS surface plot along the x- and y-spatial frequency axes. These slices are plotted on log-log axes to demonstrate the presence of 1/f noise in the imaging system.

The lower two plots in Figure 6 show single slices of the NPS taken along the *x*-spatial frequency and *y*-spatial frequency axes. For these graphs, the NPS is plotted on log-log axes. These slices are well fit by power law regression models, which appear as straight lines on the log-log plots. The characteristic exponent values of the regression models are 0.680 mm^{-1} and 0.665 mm^{-1} for the *x*- and *y*-directions, respectively. This type of behavior is ubiquitous in nature and is termed "1/*f* noise." It is caused by random fluctuations in the solid-state circuit elements comprising most electronic devices.

Task conclusions

- Though the intrinsic spatial resolution of the AO detector is itself very high (~ 10^{-9} meters) the spatial resolution of the imaging system is substantially reduced by the pixelation of the digital camera used to record the display of the AO detector for image processing and storage. The measured resolution is 400 microns.

- The noise present in the imaging system is primarily electrical in nature, as evidenced by the 1/*f* noise behavior observed in the system NPS in both the *x*- and *y*-spatial directions.

Task 3: Incorporate video camera

3.a. Incorporate the new video camera with source and AO sensor (no lens yet) and test resolution and sensitivity (U of C; mo. 6)

We have not yet incorporated the new video camera. The results above were acquired with the original video camera. Adding the video camera will be a simple modification to incorporate along with the lenses but the optimal specifications needed for the camera will depend on the properties of the fabricated lenses.

Task 4: Design, fabricate, and test acoustic lens

4.a. Determine final lens specifications based on simulation studies of whole system (U of C; mos 1-3)

Our initial plan was to fabricate an afocal triplet of acoustic lenses, as shown in Fig. 7.

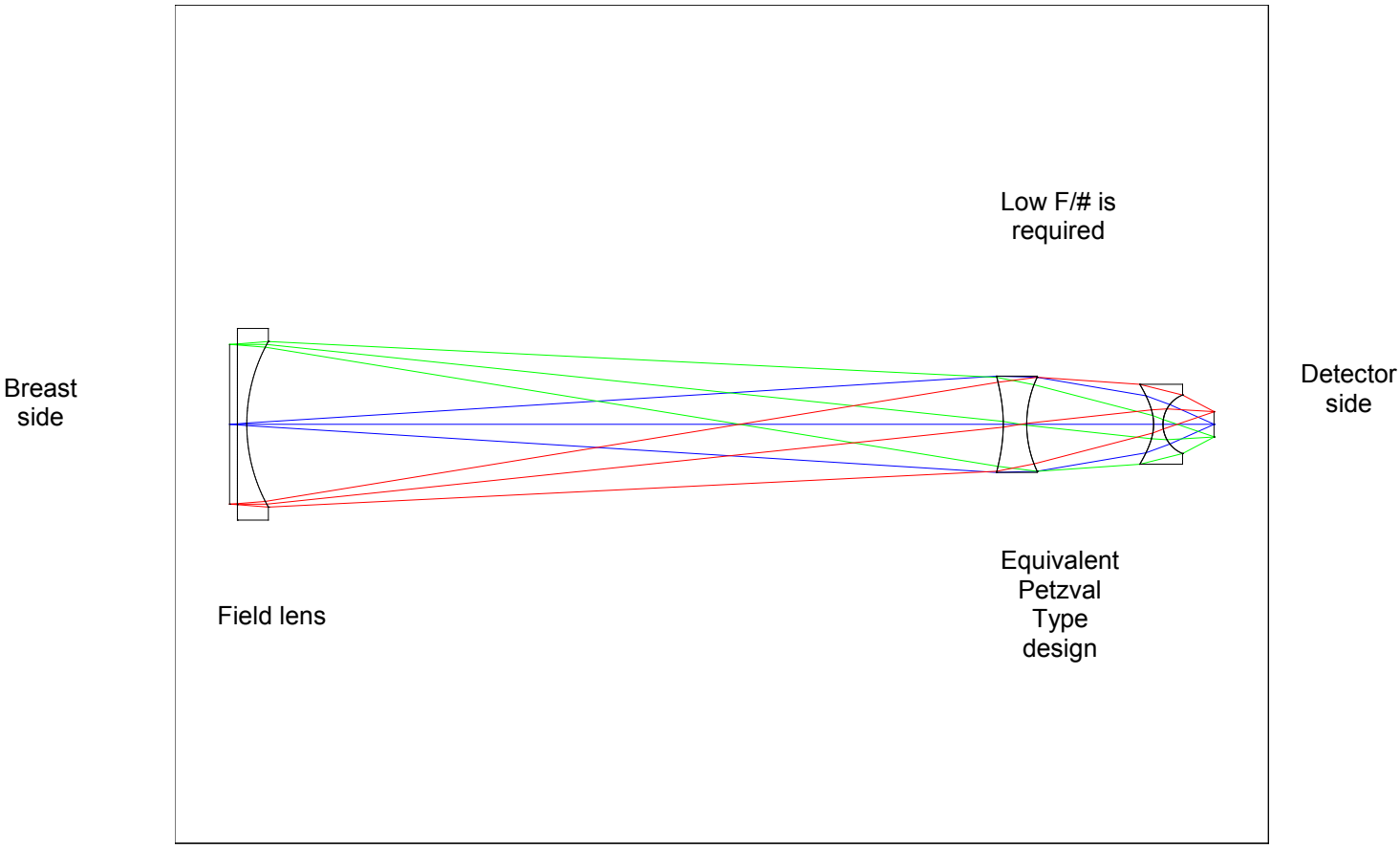

Fig. 7: Initial afocal triplet design. The acoustic attenuation in this design would have been too high.

However, initial design and simulation studies showed that because of the fast speed of the lens required (~F/3 or less), the lens thickness variation would have been about ~60 mm which would have caused unacceptable attenuation of the acoustic field.

An alternative single-lens design, shown in Fig. 8, would still have been too thick (56 mm), leading to two or three orders of magnitude of acoustic attenuation. Therefore it was decided to produce a reflective system rather than a refractive lens.

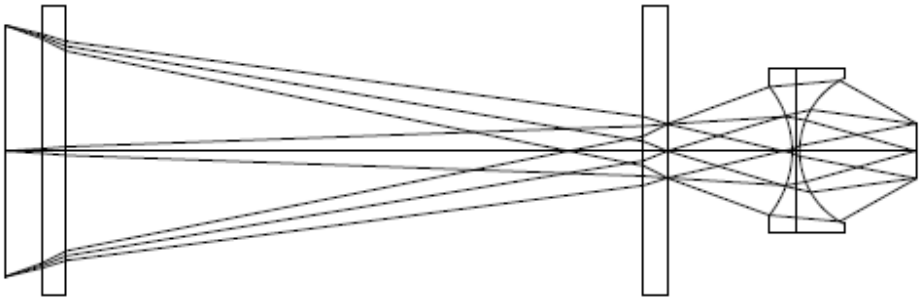

Fig 8: A single-lens design aimed at reducing acoustic attenuation still would have had unacceptable levels of it. We turned instead to a reflection-based system.

4.b. Optimize lens design using Zemax lens design software (U of C/Sasian; mos. 4-6)

We used the Zemax lens design software to optimize the mirror-based system. The schematic of the optimized mirror-based system is shown below in Fig 9.

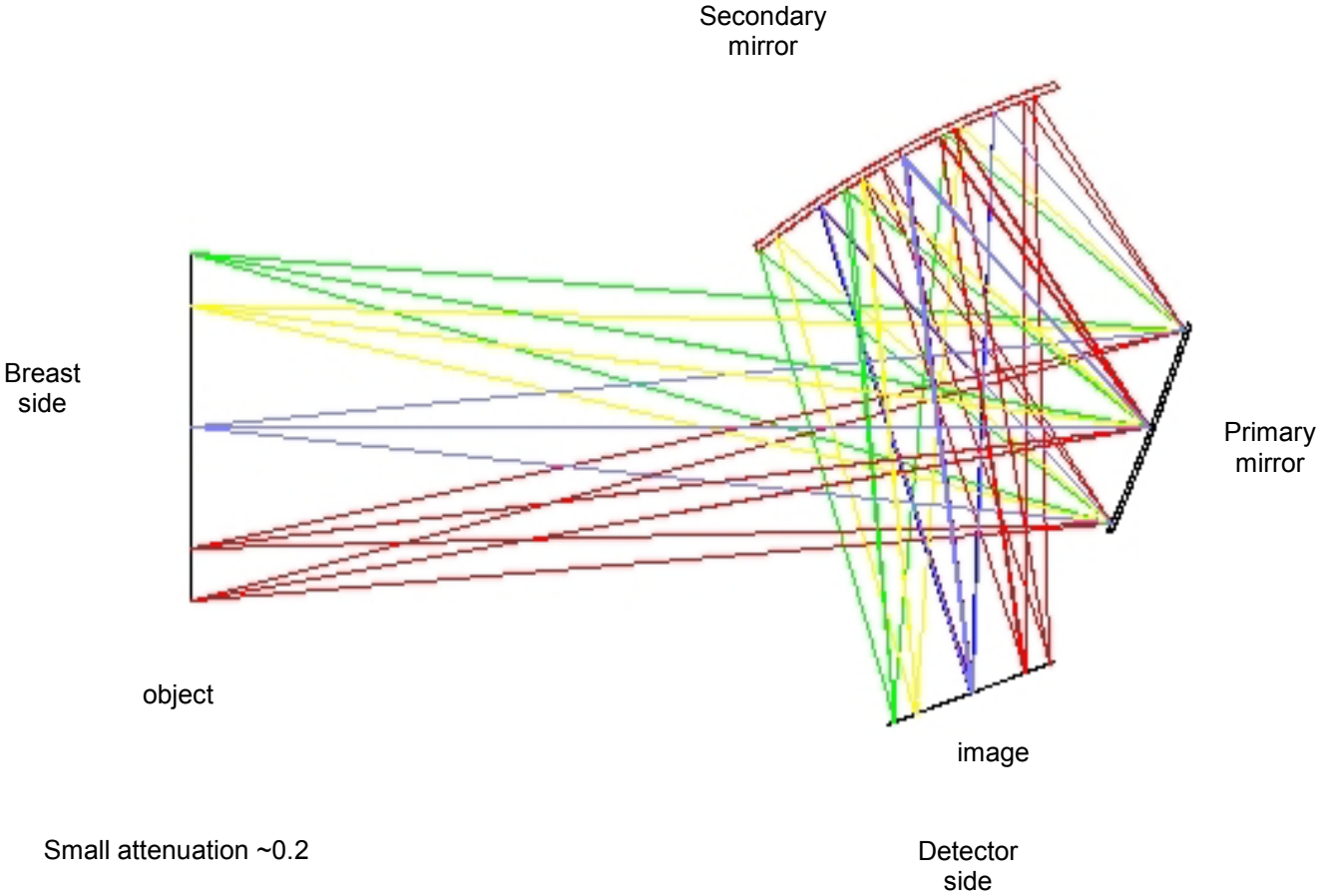

Fig 9: Cross-sectional schematic of the lens-based system.

A three-dimensional rendering is shown in Fig. 10.

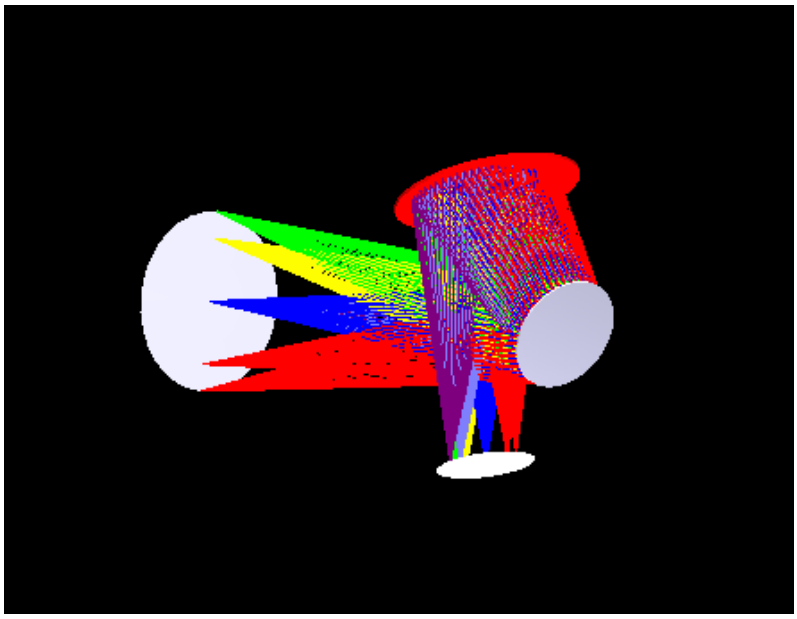

Fig 10: Three-dimensional view of the mirror-based system.

The system characteristics are as follows:

- Length: 600 mm
- Width: 310 mm
- Working F/# = 2.88
- Wavelength: 0.5 mm
- Stop aperture at primary mirror
- Other apertures for stray sound suppression are allowed
- System is plane symmetric in y-z plane
- Magnification 0.5

The primary mirror surface, which is concave, is described by

$$sag = \frac{c\left(x^2 + y^2\right)}{1 + \sqrt{1 - c^2\left(x^2 + y^2\right)}} + Ay^2 + Bx^2 y + Cy^3$$

with parameters

- c = -1/1000 mm
- A = 1.555861e-4 mm^{-1}
- B = 5.74993e-7 mm^{-2}
- C = 5.160419e-7 mm^{-2}
- Diameter = 130 mm

With these specifications, the expected performance is given in the Airy disk diagrams shown in Fig. 11.

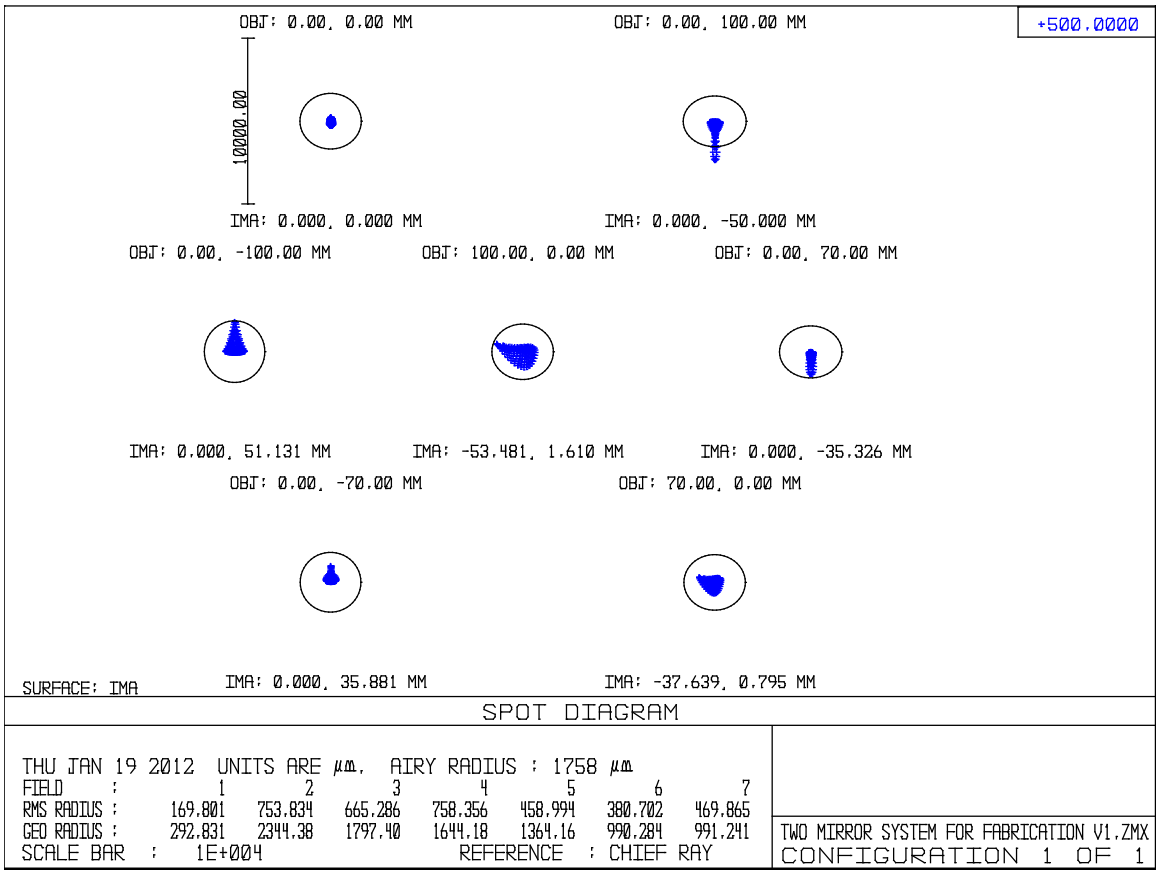

Fig 11: Airy spot diagrams showing expected performance of the lens system.

4.c. Fabricate lens (U of C/Sasian; mos. 7-8)

The mirrors are being fabricated by Lam Optics in Tucson, AZ. The secondary mirror is finished, as is the first toroidal primary. The second primary mirror is expected to be finished by June 30th.

4.d. Perform acceptance testing on lens (U of C; mo. 9)

Acceptance testing will follow final delivery of the lens, but our consultant Jose Sasian has been personally visiting the fabrication facility to observe fabrication and oversee in-house quality assurance.

Task 5: Assemble complete system

5.a. Fabricate immersion tank (Santec; mo. 9)

The dimensions of the immersion tank will be determined by the final configuration of lenses, which must await final acceptance testing of the lenses.

5.b. Assemble system (U of C; mo. 10-12)

Assembly must obviously await the delivery of the lenses.

KEY RESEARCH ACCOMPLISHMENTS:

- Successful simulation and construction of acoustic field of multielement sound source.
- Successful construction of 2-inch acousto optic (AO) sensor.
- Measurement of noise and spatial resolution properties of AO sensor coupled with existing video camera.
- Development and characterization of multiple acoustic lens systems, resulting in a very original acoustic-mirror design that should minimize acoustic attenuation relative to the original refraction-based designs.

REPORTABLE OUTCOMES:

- Poster presentation: *J.R. Rosenfield, J.S. Sandhu, J.K. Tawiah, and P.J. La Rivière,* "Evaluation of the Spatial Resolution and Noise Properties of a Prototype Transmission Ultrasound Breast Imaging System Employing an Acousto-Optic Detector," NIH NIBIB training grant symposium, June, 2012.
- Oral presentation: *J.R. Rosenfield, J.S. Sandhu, J.K. Tawiah, and P.J. La Rivière,* "Evaluation of the Spatial Resolution and Noise Properties of a Prototype Transmission Ultrasound Imaging System Employing An Acousto-Optic (AO) Detector," AAPM Annual Meeting, July, 2012.

CONCLUSION:

In summary, we have made excellent progress through the year. The simulation and construction of the sound sources and AO sensors have gone according to schedule and careful measurements have shown that the system resolution of the AO sensor coupled with the current video sensor is ~400 microns. The noise present in the imaging system is primarily electrical in nature, as evidenced by the $1/f$ noise behavior observed in the system NPS in both the x- and y-spatial directions. Our initial lens design proved impractical because of the large acoustic attenuation of the materials needed to achieve the design, but we have produced a strong alternative design based on the use of acoustic mirrors. Fabrication is going well and should be complete this summer. Integration and testing of the complete system will then proceed as originally planned.

REFERENCES:

[1] S. E. Reichenbach, S. K. Park, and R. Narayanswamy, "Characterizing digital image acquisition devices," Opt. Eng. (Bellingham) **30**, 170–177 (1991).

[2] J.M. Boone and J. A. Seibert, "An analytical edge spread function model for computer fitting and subsequent calculation of the LSF and MTF," Med Phys. 21, 1541-1545 (1994).

APPENDICES:

Appendix A provides significant detail on the acoustic simulation.

Appendix A: Details of acoustic simulation

I. Wave Equation Description

The imaging system relevant to ultrasound diffraction tomography can be treated as an inhomogeneous medium of finite size (*i.e.*, the imaged object) immersed within a lossless, homogeneous background medium providing acoustic coupling. A schematic of the measurement geometry is given in Figure 1. In the calculations that follow, all waves considered will be compressional (*i.e.*, longitudinal) in nature, as opposed to shear waves that may be present in viscous materials. Furthermore, for the sake of generality, attenuation of mechanical ultrasound energy within the imaged object will be implicitly assumed. The formalism developed here will be general enough that the case of pure scattering of an incident wave field by the object with no attenuation could just as well be described by the same equations.

For inhomogeneous media, the propagation of the acoustic pressure field in a source-free region is well known to satisfy the non-dispersive wave equation

$$\nabla^2 u(\vec{r},t) - \frac{1}{c^2(\vec{r})}\frac{\partial^2 u(\vec{r},t)}{\partial t^2} = 0, \tag{1.1}$$

where $u(\vec{r},t)$ represents the complex amplitude of the field as a function of position $\vec{r}$ and time *t*, and $c(\vec{r})$ denotes the velocity of sound as a function of position. In an inviscid medium, the wave velocity $c(\vec{r})$ is a purely real quantity, but in the presence of attenuation, the velocity becomes complex with the imaginary part reflecting attenuation in the supporting medium. The operator ∇^2 denotes the Laplacian for the spatial coordinates of the field point $\vec{r}$. In order to determine the time- and space-dependent acoustic pressure field produced by a vibrating source, we must solve (1.1) for the manner in which the

acoustic field is propagated, and we must constrain the solution to match the initial or boundary conditions defined by the problem.

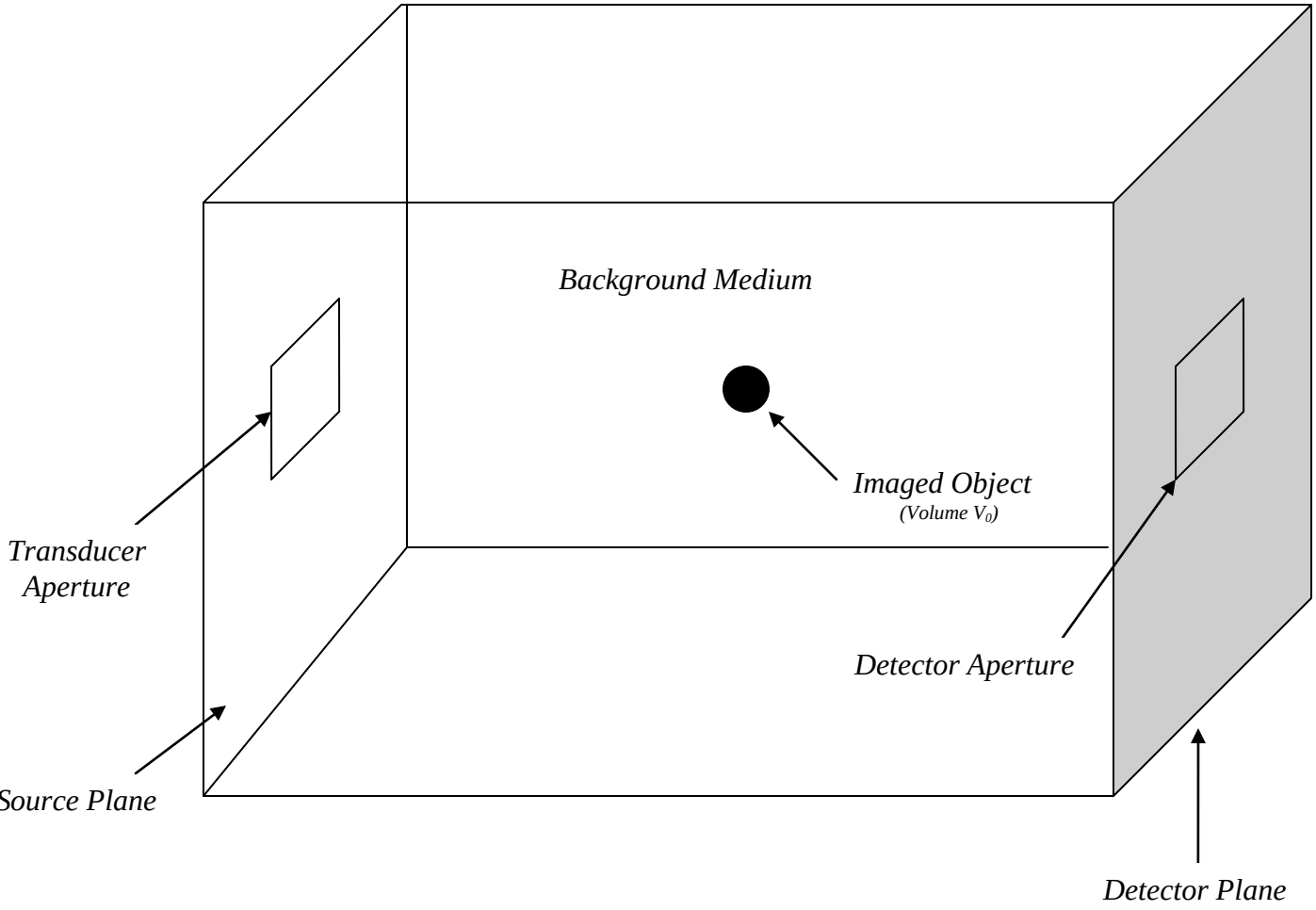

Figure 1: The measurement geometry of ultrasound diffraction tomography. The relative positions of the source and detector planes, the transducer aperture, and the imaged object are shown. The object is immersed in the lossless background medium. All waves considered will be compressional (*i.e.*, longitudinal) in nature, as opposed to shear waves that may be present in viscous materials. For the sake of generality, attenuation of mechanical ultrasound energy within the imaged object will be assumed.

Taking the Fourier transform of (1.1) with respect to time, we find that the equation conjugate to (1.1) is

$$\nabla^2 u(\vec{r},t) + k^2(\vec{r})u(\vec{r},t) = 0, \tag{1.2}$$

where $k(\vec{r})$ is the wave number as a function of position for the acoustic field having angular frequency ω. The wave number $k(\vec{r})$ is in general a complex quantity, with the imaginary part representing any

attenuation of ultrasound energy that may be present in a supporting medium and the real part specifying the phase velocity of the field at a particular position.

In the lossless background medium, $k(\vec{r})$ is a real number having the magnitude

$$k_0 = \frac{2\pi}{\lambda_0} = \frac{\omega}{c_0}, \tag{1.3}$$

where λ_0 and c_0 are the wavelength and velocity of the field in the background medium, respectively. We note that for our application, we will only consider a continuous wave (CW) acoustic source operating at a single vibrational frequency, so that ω corresponds to the frequency of the transducer used.

As (1.2) is expressed in terms of a single angular frequency ω, we may write the functional dependence of the acoustic pressure phasor $u(\vec{r},t)$ as the product of a spatially varying function and a time-harmonic factor thus:

$$u(\vec{r},t) = u(\vec{r})e^{-j\omega t}. \tag{1.4}$$

Upon substitution of this expression into (1.2), it can immediately be seen that the time dependence of the field is suppressed, and one obtains for the spatial dependence

$$\nabla^2 u(\vec{r}) + k^2(\vec{r})u(\vec{r}) = 0. \tag{1.5}$$

At this point, it is customary to write the wave number $k(\vec{r})$ in terms of the complex acoustic refractive index $n(\vec{r})$ of the inhomogeneous medium. In particular, if we denote by $n_\delta(\vec{r})$ the refractive index deviations of the scattering object from the homogeneous background medium, then we have

$$k(\vec{r}) = k_0 n(\vec{r}) = k_0(1 + n_\delta(\vec{r})), \tag{1.6}$$

where k_0 represents the wave vector magnitude in the background medium. It should be emphasized that (1.6) is valid both within and outside of the scattering object. For locations outside the scattering

object, $n_\delta(\vec{r})$ = 0 and (1.6) reduces to $k(\vec{r}) = k_0$. For completeness, we note that the acoustic refractive index may be written as

$$n(\vec{r}) = \frac{c_0}{c(\vec{r})}, \tag{1.7}$$

where c_0 again denotes the speed of sound in the homogenous background medium in which the imaged object is immersed.

To put (1.5) into a more enlightening form, we observe that if we substitute (1.6) into (1.5), add a factor of $k_0^2 u(\vec{r})$ to both sides, and rearrange, we obtain

$$(\nabla^2 + k_0^2)u(\vec{r}) = -k_0^2(n^2(\vec{r}) - 1)u(\vec{r}). \tag{1.8}$$

If we consider that the acoustic field at $\vec{r}$ consists of an incident field $u_0(\vec{r})$ present without the scattering object in place (*i.e.*, the field due solely to the output of the acoustic transducer) and a scattered field contribution $u_s(\vec{r})$ due entirely to the presence of the inhomogeneous scattering object, then we may write

$$u(\vec{r}) = u_0(\vec{r}) + u_s(\vec{r}). \tag{1.9}$$

This division of the total field $u(\vec{r})$ into an incident component and a scattered component allows us to write (1.8) as the following equivalent system of equations:

$$\begin{cases} (\nabla^2 + k_0^2)u_0(\vec{r}) = 0. \\ (\nabla^2 + k_0^2)u_s(\vec{r}) = -u(\vec{r})o(\vec{r}). \\ u(\vec{r}) = u_0(\vec{r}) + u_s(\vec{r}). \end{cases} \tag{1.10}$$

Here, $o(\vec{r})$ denotes the complex scattering object function, defined as

$$o(\vec{r}) = k_0^2(n^2(\vec{r}) - 1). \tag{1.11}$$

Note that $o(\vec{r})$ is defined both within and outside of the scattering object, although it vanishes everywhere outside of the scattering object since according to (1.6), $n(\vec{r})$ = 1 in the homogeneous

background medium. A final technical point worth noting is that the acoustic refractive index function $n(\vec{r})$ is in general a complex-valued quantity. For lossless media, $n(\vec{r})$ is real. The complex nature of the refractive index for attenuating media plays an extremely important role in ultrasound diffraction tomography using measurements of field intensity.

II. The Angular Spectrum Method

The physical significance of $u_0(\vec{r})$ can be particularly well understood by noting that the differential equation in (1.10) for the incident field $u_0(\vec{r})$,

$$(\nabla^2 + k_0^2)u_0(\vec{r}) = 0, \tag{1.12}$$

is the homogeneous Helmholtz equation for the acoustic pressure field in a uniform, lossless medium characterized by a wave vector of magnitude k_0. The solution to this equation is simply the solution to the wave equation in the absence of the scattering object, which is what we intended $u_0(\vec{r})$ to represent when we defined the total field $u(\vec{r})$ according to (1.9). The solution to (1.12) for the incident field $u_0(\vec{r})$ can easily be verified through substitution to be a plane wave

$$u_0(\vec{r}) = e^{j\vec{k}\cdot\vec{r}} \tag{1.13}$$

moving in an arbitrary direction specified by the propagation vector

$$\vec{k} = (k_x, k_y, k_z), \tag{1.14}$$

which has the magnitude $\left|\vec{k}\right| = \sqrt{k_x^2 + k_y^2 + k_z^2} = k_0$ appropriate for the background medium.

Equation (1.13), together with the condition $\left|\vec{k}\right| = \sqrt{k_x^2 + k_y^2 + k_z^2} = k_0$, provides the generic form of the plane wave solution to the homogeneous Helmholtz equation (1.12) for the incident acoustic field. Because (1.12) is a linear differential equation, a superposition of plane wave solutions each

having the form given in (1.13) and subject to $\left|\vec{k}\right| = \sqrt{k_x^2 + k_y^2 + k_z^2} = k_0$ is therefore also a solution. In other words, we can construct an arbitrary wave field that satisfies (1.12) from a sum of plane waves all having the same wave vector magnitude k_0 but propagating in different directions. This observation forms the mathematical basis of the so-called angular spectrum method (ASM) for solving the homogeneous Helmholtz equation subject to a particular set of boundary conditions.

In three dimensions, the ASM enables the incident acoustic pressure field to be determined throughout all space from knowledge of the field on only a single plane. To understand how this is possible, we consider our ultrasound tomography system to consist of a square piston transducer plate of dimensions $[a, a]$ centered on the *z*-axis and lying entirely in the *x*-*y* plane. We suppose that this transducer is producing an acoustic wave field only in the positive *z*-direction. In the plane $z = 0$ (*i.e.*, on the transducer surface), the incident acoustic pressure field $u_0(\vec{r})$ can be decomposed via the non-unitary, two-dimensional inverse Fourier transform relation

$$u_0(x, y, z = 0) = \frac{1}{4\pi^2} \int_{-\infty}^{\infty} \int_{-\infty}^{\infty} \alpha(k_x, k_y : z = 0) e^{j(k_x x + k_y y)} dk_x dk_y, \qquad (1.15)$$

where $\alpha(k_x, k_y : z = 0)$ denotes the spatial frequency spectral density function required to synthesize the known pressure distribution $u_0(x, y, z = 0)$ from two-dimensional plane waves of the form $e^{j(k_x x + k_y y)}$. Equation (1.15) expresses the so-called angular spectrum decomposition of the incident pressure field $u_0(\vec{r})$ on the plane $z = 0$. That such a decomposition can be achieved is a fundamental result of Fourier analysis. Provided $u_0(x, y, z = 0)$ is known for all *x* and *y* in the plane $z = 0$, we can determine the precise functional form of $\alpha(k_x, k_y : z = 0)$ required to synthesize this spatial pressure distribution simply by inverting (1.15) thus:

$$\alpha(k_x, k_y : z = 0) = \int_{-\infty}^{\infty} \int_{-\infty}^{\infty} u_0(x, y, z = 0) e^{-j(k_x x + k_y y)} dx dy. \qquad (1.16)$$

We note that each two-dimensional plane wave present in the summation of (1.15) can be attributed to one of the valid plane wave solutions (1.13) to the homogeneous Helmholtz wave equation (1.12). In particular, we observed earlier that any plane wave of the form

$$u_0(\vec{r}) = e^{j(k_x x + k_y y + k_z z)} \tag{1.17}$$

and subject to the condition

$$k_0^2 = k_x^2 + k_y^2 + k_z^2 \tag{1.18}$$

satisfies the differential equation (1.12). Thus, we see that each plane wave of the form $e^{j(k_x x + k_y y)}$ appearing in the summation of (1.15) can be associated with a valid plane wave solution $e^{j(k_x x + k_y y + k_z z)}$ to the homogeneous Helmholtz equation, where the value of k_z is determined uniquely from the values of k_x and k_y according to

$$k_z = \sqrt{k_0^2 - k_x^2 - k_y^2}. \tag{1.19}$$

In (1.19), we have restricted values of k_z to be positive because the transducer for our system produces an acoustic field only in the positive *z*-direction.

Once the decomposition of the incident acoustic field in the transducer plane ($z = 0$) has been achieved via (1.16), we can determine the field in any other parallel plane $z > 0$ in the following manner. Each plane wave $e^{j(k_x x + k_y y + k_z z)}$ required at $z = 0$ to synthesize $u_0(x, y, z = 0)$ according to (1.15) will undergo a phase shift as it propagates from the transducer plane to the plane of interest. The change in phase in passing from the point (x, y, 0) in the transducer plane to the point (x, y, z) in the measurement plane is simply $k_z z$. Thus, the complex amplitude of the plane wave component $e^{j(k_x x + k_y y)}$ of the total acoustic field at $z = 0$ is related to its complex amplitude at $z > 0$ by the factor $e^{jk_z z}$. This is just another way of saying that for a given plane wave component of the total acoustic field,

$$u_0(x, y, z) = \alpha\, e^{j(k_x x + k_y y + k_z z)} = \left(\alpha\, e^{j(k_x x + k_y y)}\right) e^{jk_z z} = u_0(x, y, 0) e^{jk_z z}. \tag{1.20}$$

Accounting for the change in phase of each plane wave component of the angular spectrum decomposition of $u_0(x, y, z = 0)$ in propagating from the plane $z = 0$ to any plane $z > 0$, we therefore have for the acoustic pressure field $u_0(x, y, z)$

$$u_0(x, y, z) = \frac{1}{4\pi^2} \int_{-\infty}^{\infty} \int_{-\infty}^{\infty} \alpha(k_x, k_y : z = 0) e^{j(k_x x + k_y y + k_z z)} dk_x dk_y, \qquad (1.21)$$

where again

$$k_z = \sqrt{k_0^2 - k_x^2 - k_y^2}, \qquad (1.22)$$

as required by the homogeneous Helmholtz equation for the background medium. Equation (1.21) allows us to calculate the incident acoustic field at any point (x, y, z) by determining $\alpha(k_x, k_y : z = 0)$, which itself requires knowledge only of $u_0(x, y, z = 0)$. We note that we can write (1.21) in terms of the spatial frequency spectral density function $\alpha(k_x, k_y : z)$ for any plane of constant z, not necessarily $z = 0$, by observing that

$$\alpha(k_x, k_y : z) = \alpha(k_x, k_y : z = 0) e^{jk_z z}. \qquad (1.23)$$

Then (1.21) assumes the recognizable form of a simple two-dimensional inverse Fourier transform in the plane z:

$$u_0(x, y, z) = \frac{1}{4\pi^2} \int_{-\infty}^{\infty} \int_{-\infty}^{\infty} \alpha(k_x, k_y : z) e^{j(k_x x + k_y y)} dk_x dk_y. \qquad (1.24)$$

Before applying the ASM to a rectangular piston transducer having a known surface velocity profile, it is important to consider two limiting cases for the z-component k_z of the propagation vector $\vec{k} = (k_x, k_y, k_z)$. We mentioned above that for each plane wave in the expansion (1.21), the value of k_z for that component of the expansion is determined from the corresponding values of k_x and k_y according to (1.22). Because the integration limits in (1.21) run from $-\infty$ to $+\infty$, we see that for

values of k_x and k_y such that $k_0^2 < k_x^2 + k_y^2$, the radical in (1.22) becomes complex and k_z is pure imaginary. Under this circumstance, the plane wave solution to the Helmholtz equation becomes the so-called evanescent wave. The complex nature of k_z for evanescent waves leads to a real, attenuating component that causes the amplitudes of these solutions to decay exponentially. Though they are valid solutions to the wave equation, evanescent waves carry no net energy and can be considered a non-physical outcome of the ASM related to boundary condition matching. Evanescent waves decay rapidly when moving away from any boundaries present, and their influence can often be ignored at distances from boundaries exceeding ten times the acoustic wavelength. On the other hand, for $k_0^2 > k_x^2 + k_y^2$, k_z is real and the corresponding solution to the Helmholtz equation remains a plane wave propagating in the direction of positive *z* without exhibiting evanescent decay.

III. Solution for the Incident Field $u_0(\vec{r})$

We will now apply the ASM outlined above to our square transducer plate having a known velocity profile. For a planar acoustic source radiating into an unbounded, lossless background medium, solving the Helmholtz wave equation (1.12) for the incident field requires matching the boundary condition for the pressure field on the acoustic source plane only. Since there are no other physical boundaries present, the value of the field at all other points in the homogeneous medium is determined by the movement of the wave field output from the source plane through the medium as required by the propagation equation (1.1). One could nominally require that the magnitude of the acoustic pressure field vanishes at an infinite distance from the transducer surface. We will see, however, that this condition will be satisfied by the solution we obtain by only considering the boundary condition on the transducer plane. We discussed in the previous section how the ASM enables us to achieve this required boundary condition on the source plane, and that the total acoustic field can be determined on any other

parallel plane simply by propagating the plane wave solutions of the Helmholtz equation from the source plane to the plane of interest.

As mentioned previously, our analysis will be confined to an acoustic source consisting of a single square transducer plate of dimensions $[a, a]$ centered on the *z*-axis and lying entirely in the *x*-*y* plane. We will assume CW excitation of the source at a single vibrational frequency ω. The source will be embedded in an ideal rigid baffle such that there is no vibration of the transducer plane outside of the transducer aperture dimensions $[a, a]$. We can therefore write for the surface velocity of any point in the transducer plane

$$v_z(x, y, z = 0 : t) = v_0 \text{rect}\left(\frac{x}{a}\right)\text{rect}\left(\frac{y}{a}\right)e^{-j\omega t}, \tag{1.25}$$

where v_0 is a constant indicating the velocity amplitude of the oscillations and the subscript z reminds us that this is the velocity component perpendicular to the plane $z = 0$. Equation (1.25) is known as the vibration velocity waveform of the acoustic source aperture, and in particular, the function

$$\xi(x, y) = \text{rect}\left(\frac{x}{a}\right)\text{rect}\left(\frac{y}{a}\right), \tag{1.26}$$

describing the spatial dependence of the velocity waveform is known as the apodization function. For clarity, it should be realized that for a moveable surface enclosing a fluid acoustic medium, kinematic boundary conditions require that the component of the fluid velocity normal to the surface equals the velocity of the bounding surface in the same direction. In other words, (1.25) equally well represents either the velocity of the vibrating transducer surface or the component of the fluid velocity normal to the transducer surface in the plane $z = 0$.

Solution of the Helmholtz equation (1.12) requires that either the acoustic pressure on the boundary surface S_0 or the normal component of the medium particle velocity on the boundary surface be specified. Specification of the normal component of the medium particle velocity distribution in the

transducer plane constitutes the so-called Neumann boundary condition for the differential equation (1.12), whereas specification of the pressure distribution on this plane constitutes the Dirichlet boundary condition. As written, (1.24) is expressed in terms of the pressure distribution in the transducer plane and is therefore related to the Dirichlet boundary condition. However, the Neumann boundary condition is more directly related to the velocity waveform of the transducer aperture, and therefore it has proven advantageous to express (1.24) in terms of the Neumann condition. This can be achieved by first taking the two-dimensional Fourier transform of (1.24) with respect to *x* and *y* to obtain

$$\alpha(k_x, k_y : z) = \int_{-\infty}^{\infty}\int_{-\infty}^{\infty} u_0(x, y, z) e^{-j(k_x x + k_y y)} dxdy. \tag{1.27}$$

Equation (1.27) can equally well be expressed in terms of the velocity potential function $\Phi_0(\vec{r}, t)$ for the incident field, which for an inviscid medium is related to the incident acoustic pressure field $u_0(\vec{r}, t)$ according to

$$u_0(\vec{r}, t) = \rho_0 \frac{\partial \Phi_0(\vec{r}, t)}{\partial t}. \tag{1.28}$$

Here, ρ_0 is the mass density of the uniform, lossless background medium. With $u_0(\vec{r}, t) = u_0(\vec{r}) e^{-j\omega t}$ as in (1.4), we therefore have

$$\Phi_0(\vec{r}, t) = \frac{-1}{j\omega\rho_0} u_0(\vec{r}) e^{-j\omega t} = \Phi_0(\vec{r}) e^{-j\omega t}. \tag{1.29}$$

Canceling the harmonic factor $e^{-j\omega t}$ from both sides of (1.29) that characterizes the time dependence of $\Phi_0(\vec{r}, t)$ and $u_0(\vec{r}, t)$, we have

$$\Phi_0(\vec{r}) = \frac{-1}{j\omega\rho_0} u_0(\vec{r}). \tag{1.30}$$

Substitution of (1.30) for $u_0(\vec{r})$ in (1.27) gives

$$\alpha(k_x,k_y:z)=-j\omega\rho_0\int_{-\infty}^{\infty}\int_{-\infty}^{\infty}\Phi_0(x,y,z)e^{-j(k_xx+k_yy)}dxdy. \tag{1.31}$$

Differentiation of (1.31) with respect to z gives

$$\frac{\partial\alpha(k_x,k_y:z)}{\partial z}=-j\omega\rho_0\int_{-\infty}^{\infty}\int_{-\infty}^{\infty}\frac{\partial\Phi_0(x,y,z)}{\partial z}e^{-j(k_xx+k_yy)}dxdy, \tag{1.32}$$

while differentiation of (1.23) with respect to z similarly gives

$$\frac{\partial\alpha(k_x,k_y:z)}{\partial z}=\alpha(k_x,k_y:z=0)\frac{\partial\left(e^{jk_zz}\right)}{\partial z}=jk_z\alpha(k_x,k_y:z=0)e^{jk_zz}. \tag{1.33}$$

Equating (1.32) and (1.33) and evaluating in the transducer plane at $z = 0$ yields

$$jk_z\alpha(k_x,k_y:z=0)=j\omega\rho_0\int_{-\infty}^{\infty}\int_{-\infty}^{\infty}\left[\frac{-\partial\Phi_0(x,y,z)}{\partial z}\right]_{z=0}e^{-j(k_xx+k_yy)}dxdy. \tag{1.34}$$

Since the fluid particle velocity vector $\vec{v}(\vec{r},t)$ at any point in the background medium and the velocity potential $\Phi_0(\vec{r},t)$ at the same position and time are related according to

$$\vec{v}(\vec{r},t)=-\vec{\nabla}\Phi(\vec{r},t), \tag{1.35}$$

we can recognize the factor

$$\left[\frac{-\partial\Phi_0(x,y,z)}{\partial z}\right]_{z=0} \tag{1.36}$$

appearing in the integrand of (1.34) as the component of the fluid particle velocity normal to the transducer surface in the plane $z = 0$. In other words, using (1.25) and (1.36), we have

$$v_z(x,y,z=0)=\left[\frac{-\partial\Phi_0(x,y,z)}{\partial z}\right]_{z=0}, \tag{1.37}$$

whence (1.34) becomes

$$jk_z\alpha(k_x,k_y:z=0)=j\omega\rho_0\int_{-\infty}^{\infty}\int_{-\infty}^{\infty}v_z(x,y,z=0)e^{-j(k_xx+k_yy)}dxdy. \tag{1.38}$$

Solving (1.38) for $\alpha(k_x, k_y : z = 0)$, we have

$$\alpha(k_x, k_y : z = 0) = \frac{\omega\rho_0}{k_z} \int_{-\infty}^{\infty}\int_{-\infty}^{\infty} v_z(x, y, z = 0) e^{-j(k_x x + k_y y)} dxdy, \qquad (1.39)$$

which expresses the spatial frequency spectral density function for the incident acoustic field in the plane $z = 0$ in terms of the component of the fluid velocity normal to the transducer surface in that same plane. Insertion of the spatial frequency spectral density function of (1.39) into (1.21),

$$u_0(x, y, z) = \frac{1}{4\pi^2} \int_{-\infty}^{\infty}\int_{-\infty}^{\infty} \alpha(k_x, k_y : z = 0) e^{j(k_x x + k_y y + k_z z)} dk_x dk_y, \qquad (1.40)$$

gives the acoustic pressure field $u_0(x, y, z)$ everywhere.

For the transducer surface velocity waveform of (1.25), the spatial frequency spectral density function for the incident acoustic field in the plane $z = 0$ is according to (1.39),

$$\alpha(k_x, k_y : z = 0) = \frac{\omega\rho_0 v_0}{k_z} \int_{-\infty}^{\infty}\int_{-\infty}^{\infty} \text{rect}\left(\frac{x}{a}\right)\text{rect}\left(\frac{y}{a}\right) e^{-j(k_x x + k_y y)} dxdy. \qquad (1.41)$$

We can immediately recognize the integral in (1.41) as the Fourier transform of the two-dimensional rectangle function of dimensions $[a, a]$ in x and y. The result of this transformation is well known to give a product of sinc functions thus:

$$\alpha(k_x, k_y : z = 0) = \frac{\omega\rho_0 v_0 a^2}{k_z} \text{sinc}\left(\frac{k_x a}{2}\right)\text{sinc}\left(\frac{k_y a}{2}\right), \qquad (1.42)$$

where $\text{sinc}(x) = \sin(x)/x$. Inserting (1.42) into (1.40) gives for the incident acoustic field

$$u_0(x, y, z) = \frac{\omega\rho_0 v_0 a^2}{4\pi^2} \int_{-\infty}^{\infty}\int_{-\infty}^{\infty} \frac{1}{k_z} \text{sinc}\left(\frac{k_x a}{2}\right)\text{sinc}\left(\frac{k_y a}{2}\right) e^{j(k_x x + k_y y + k_z z)} dk_x dk_y. \qquad (1.43)$$

It is important to realize that the factors in (1.43) involving k_z cannot be pulled out of the integrand since k_z depends on k_x and k_y according to (1.19). We should therefore write the preceding expression more explicitly as

$$u_0(x,y,z) = \frac{\omega\rho_0 v_0}{4\pi^2}\int_{-\infty}^{\infty}\int_{-\infty}^{\infty}\left[\frac{e^{j\left(\sqrt{k_0^2-k_x^2-k_y^2}\right)z}}{\sqrt{k_0^2-k_x^2-k_y^2}}a^2\mathrm{sinc}\left(\frac{k_x a}{2}\right)\mathrm{sinc}\left(\frac{k_y a}{2}\right)\right]e^{j(k_x x+k_y y)}dk_x dk_y. \quad (1.44)$$

Equation (1.44) is the non-unitary inverse Fourier transform of the bracketed function multiplied by the pre-factor $\omega\rho_0 v_0$. Thus, we write (1.44) more succinctly as

$$u_0(x,y,z) = \omega\rho_0 v_0 F^{-1}\left\{\frac{e^{j\left(\sqrt{k_0^2-k_x^2-k_y^2}\right)z}}{\sqrt{k_0^2-k_x^2-k_y^2}}a^2\mathrm{sinc}\left(\frac{k_x a}{2}\right)\mathrm{sinc}\left(\frac{k_y a}{2}\right)\right\}, \quad (1.45)$$

where $F^{-1}\{\ \}$ denotes the two-dimensional inverse Fourier transform with respect to k_x and k_y of the function in brackets. Invoking the convolution-multiplication theorem, we can write (1.45) equivalently as

$$u_0(x,y,z) = \omega\rho_0 v_0\left[F^{-1}\left\{\frac{e^{j\left(\sqrt{k_0^2-k_x^2-k_y^2}\right)z}}{\sqrt{k_0^2-k_x^2-k_y^2}}\right\} ** F^{-1}\left\{a^2\mathrm{sinc}\left(\frac{k_x a}{2}\right)\mathrm{sinc}\left(\frac{k_y a}{2}\right)\right\}\right], \quad (1.46)$$

where $**$ denotes two-dimensional convolution with respect to the spatial variables x and y. The inverse Fourier transform of the product of sinc functions is simply the apodization function (1.26) of the transducer velocity waveform:

$$F^{-1}\left\{a^2\mathrm{sinc}\left(\frac{k_x a}{2}\right)\mathrm{sinc}\left(\frac{k_y a}{2}\right)\right\} = \mathrm{rect}\left(\frac{x}{a}\right)\mathrm{rect}\left(\frac{y}{a}\right). \quad (1.47)$$

Examining the first term in brackets in (1.46), we see that

$$F^{-1}\left\{\frac{e^{j\left(\sqrt{k_0^2-k_x^2-k_y^2}\right)z}}{\sqrt{k_0^2-k_x^2-k_y^2}}\right\} = \frac{1}{4\pi^2}\int_{-\infty}^{\infty}\int_{-\infty}^{\infty}\frac{e^{j\left(\sqrt{k_0^2-k_x^2-k_y^2}\right)z}}{\sqrt{k_0^2-k_x^2-k_y^2}}e^{j(k_x x+k_y y)}dk_x dk_y. \quad (1.48)$$

Combining the exponential factors in (1.48), we have

$$F^{-1}\left\{\frac{e^{j\left(\sqrt{k_0^2-k_x^2-k_y^2}\right)z}}{\sqrt{k_0^2-k_x^2-k_y^2}}\right\} = \frac{1}{4\pi^2}\int_{-\infty}^{\infty}\int_{-\infty}^{\infty}\frac{e^{j\left(k_x x+k_y y+z\sqrt{k_0^2-k_x^2-k_y^2}\right)}}{\sqrt{k_0^2-k_x^2-k_y^2}}dk_x dk_y. \quad (1.49)$$

As any spherical wave can be decomposed in a plane wave basis, equation (1.49) represents the plane wave decomposition of a spherical wave centered at the origin and characterized by a wave vector of magnitude k_0. In particular, we have for $z \geq 0$,

$$\frac{1}{4\pi^2}\int_{-\infty}^{\infty}\int_{-\infty}^{\infty}\frac{e^{j\left(k_x x + k_y y + z\sqrt{k_0^2 - k_x^2 - k_y^2}\right)}}{\sqrt{k_0^2 - k_x^2 - k_y^2}}dk_x dk_y = \frac{1}{j2\pi}\left[\frac{e^{jk_0 r}}{r}\right], \tag{1.50}$$

where $r = \sqrt{x^2 + y^2 + z^2}$ is the Euclidean distance from the origin to the point (x, y, z). Combing (1.46), (1.47), and (1.50), we have for the incident acoustic pressure field

$$u_0(x, y, z) = -j\rho_0 v_0 f\left[\frac{e^{jk_0 r}}{r} * *\text{rect}\left(\frac{x}{a}\right)\text{rect}\left(\frac{y}{a}\right)\right], \tag{1.51}$$

where we have used the relationship $\omega = 2\pi f$ between the angular frequency of the transducer vibration and the corresponding linear frequency. Expression of $u_0(x, y, z)$ in terms of the linear frequency f is advantageous since ultrasound transducers are generally always referred to in terms of linear frequency in MHz. With the exception of the velocity amplitude v_0, all quantities appearing in (1.51) can easily be determined from knowledge of the acoustic background medium and the transducer employed for measurements.

Equation (1.51) represents the sought-after expression for the spatial dependence of the incident acoustic pressure field output by a monochromatic transducer plate of dimensions $[a, a]$ centered on the z-axis and lying entirely in the plane $z = 0$. It suggests that the incident field is given quite simply by the convolution of a spherical wave with a two-dimensional indicator function describing the transducer aperture. In reality, (1.51) is simply a restatement of Huygens' Principle, which considers that each infinitesimal transducer surface element acts as an acoustic monopole emitting a spherical wave. This can be seen by writing the convolution of (1.51) explicitly:

$$u_0(x,y,z) = -j\rho_0 v_0 f \int_{-\infty}^{\infty}\int_{-\infty}^{\infty} \mathrm{rect}\left(\frac{\xi}{a}\right)\mathrm{rect}\left(\frac{\eta}{a}\right)\frac{e^{jk_0\sqrt{(x-\xi)^2+(y-\eta)^2+z^2}}}{\sqrt{(x-\xi)^2+(y-\eta)^2+z^2}}\,d\xi d\eta. \quad (1.52)$$

Since the rect function is nonzero only when the absolute value of its argument is $\leq 1/2,$ we can write (1.52) as

$$u_0(x,y,z) = -j\rho_0 v_0 f \int_{-a/2}^{a/2}\int_{-a/2}^{a/2} \frac{e^{jk_0\sqrt{(x-\xi)^2+(y-\eta)^2+z^2}}}{\sqrt{(x-\xi)^2+(y-\eta)^2+z^2}}\,d\xi d\eta. \quad (1.53)$$

Because $\sqrt{(x-\xi)^2+(y-\eta)^2+z^2}$ is the Euclidean distance between an arbitrary point $(\xi,\eta,0)$ on the planar transducer surface and a field point of interest (*x*, *y*, *z*), the surface integral in (1.53) represents the summation at the field point of an infinite number of spherical waves, each of which is centered on a different infinitesimal surface element of the transducer. We note that the integration limits in (1.53) run from $[-a/2, a/2]$ in both the ξ and η directions (*i.e.*, the integration is performed over the entire transducer surface). According to Huygens' Principle, the total field output by a continuous source distribution is given by the superposition of all spherical waves emitted by the infinitesimal acoustic monopoles composing the source. This superposition leads to regions of constructive and destructive interference between interfering spherical waves and manifests itself in observable patterns of diffraction. Ultimately, the cause of these observed interference patterns is traceable to differences in path length traveled by individual, coherent spherical waves in propagating from their respective source centers on the transducer surface to a field point of interest.

While (1.51) in the form of (1.53) is exactly equal to the well-known Rayleigh-Sommerfeld diffraction integral for a square transducer plate of dimensions $[-a, a]$ centered at *z* = 0 and excited by the velocity waveform (1.25), the efficiency with which modern computer programs can perform convolution operations makes the insight provided by the angular spectrum derivation well worth the effort. Figure 2 below shows the normalized in-plane incident acoustic intensity distribution for a 3" by 3" square transducer piston operating at a CW frequency of 3.35 MHz. The pressure field intensity is

depicted in the plane parallel to the transducer surface at a distance of 2", and a background medium of water has been assumed. At 3.35 MHz, the attenuation coefficient of water is only ~ 0.02 dB/cm, so water represents a very good approximation to a truly inviscid background medium. We note that the square modulus of the complex field given by (1.51) is plotted in Figure 2.

Figure 3 below presents the same information as Figure 2 but shows the spatial distribution of acoustic intensity looking at the plane of interest head-on. For a planar detector positioned 2" from the transducer surface, one would expect to observe this type of diffraction pattern for an image acquired with no scattering object present.

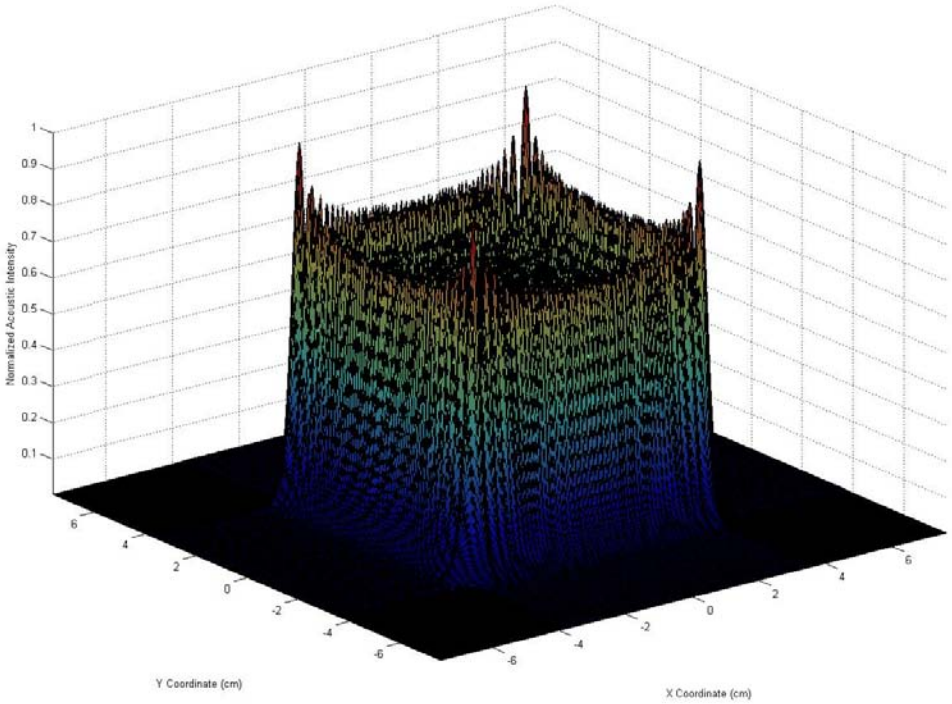

Figure 2: The normalized in-plane acoustic intensity distribution for a 3” by 3” square transducer piston operating at a CW frequency of 3.35 MHz. The pressure field intensity is depicted in the plane parallel to the transducer surface at a distance of 2”, and a background medium of water has been assumed. We note that the square modulus of the acoustic pressure field calculated in (1.51) is plotted.

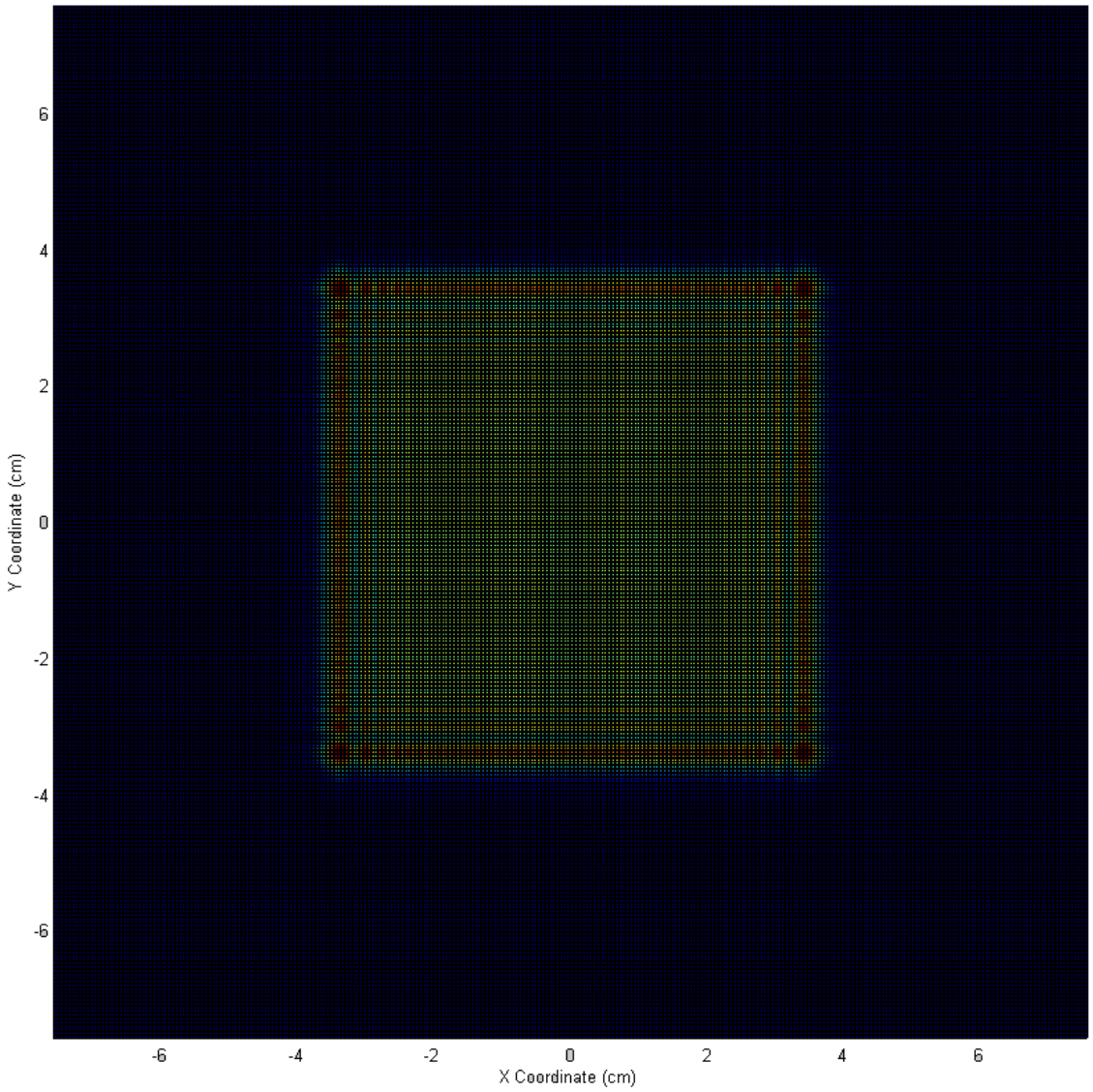

Figure 3: This figure presents the same information as Figure 1 but shows the spatial distribution of acoustic intensity looking at the plane of interest head-on. For a planar detector positioned 2" from the transducer surface, one would expect to observe this type of diffraction pattern for an image acquired with no scattering object present.

We observe finally that the complete incident acoustic field, including both time and spatial dependence, is given by the product of (1.51) with the time-harmonic factor $e^{-j\omega t}$ thus:

$$u_0(\vec{r},t) = u_0(\vec{r})e^{-j\omega t} = -j\rho_0 v_0 f\left[\frac{e^{jk_0 r}}{r} * *\text{rect}\left(\frac{x}{a}\right)\text{rect}\left(\frac{y}{a}\right)\right]e^{-j\omega t}. \qquad (1.54)$$

Due to the linearity of the acoustic field, for any transducer array composed of multiple square transducers each of dimension $[a,a]$ and vibrating in unison at angular frequency ω, the total field

produced by such an array is given quite simply by appropriately shifting and adding the individual transducer outputs as described by (1.54).

IV. Solution for the Scattered Field $u_s(\vec{r})$

The equation for the scattered field component $u_s(\vec{r})$ from (1.10),

$$(\nabla^2 + k_0^2)u_s(\vec{r}) = -u(\vec{r})o(\vec{r}), \tag{1.55}$$

is an inhomogeneous Helmholtz equation with a source term on the right-hand side due to the presence of the complex object function $o(\vec{r})$. Thus, as expected, the scattered field $u_s(\vec{r})$ arises because of the perturbing influence of the scattering object immersed in the background medium. Equation (1.55) cannot be solved directly for the scattered field, but a solution can be written in terms of the so-called Green's function for the above differential equation. In particular, the Green's function, which we denote by $g(\vec{r}|\vec{r}')$, is a solution to the related differential equation

$$(\nabla^2 + k_0^2)g(\vec{r}|\vec{r}') = -\delta(\vec{r} - \vec{r}'), \tag{1.56}$$

in which the source term $u(\vec{r})o(\vec{r})$ of (1.55) has been replaced by the Dirac delta function $\delta(\vec{r} - \vec{r}')$. Physically, the function $\delta(\vec{r} - \vec{r}')$ represents a single point inhomogeneity located at position $\vec{r}'$, and therefore the Green's function $g(\vec{r}|\vec{r}')$ represents the scattered wave field at $\vec{r}$ due to the point inhomogeneity at $\vec{r}'$. In this sense, the Green's function is analogous to the impulse response function of linear systems theory. For a background medium of infinite extent, the appropriate three-space Green's function satisfying (1.56) is given by

$$g(\vec{r}|\vec{r}') = \frac{e^{jk_0|\vec{r}-\vec{r}'|}}{4\pi|\vec{r} - \vec{r}'|}. \tag{1.57}$$

Since (1.57) is a function only of the position vector difference $\vec{r} - \vec{r}'$, we write the functional dependence of $g(\vec{r}|\vec{r}')$ more explicitly as

$$g(\vec{r} - \vec{r}') = \frac{e^{jk_0|\vec{r}-\vec{r}'|}}{4\pi|\vec{r} - \vec{r}'|}. \tag{1.58}$$

Equation (1.58) corresponds to the outgoing scattered field generated by a harmonic point source at $\vec{r}'$ that radiates a spherical wave; the wave amplitude falls off as the inverse of the distance between the point source at $\vec{r}'$ and the field point $\vec{r}$ of interest.

It should be emphasized that the Green's function presented in (1.58) corresponds to the unbounded case in which an acoustic monopole radiates a scattered spherical wave into an infinite background medium. In practice, the background medium is confined by rigid barriers that are capable of reflecting acoustic waves back through the medium. Thus, in the case of a bounded medium, the free space Green's function (1.58) may not provide an accurate solution for the scattered wave field, and a different form of the Green's function may be needed to account for reflections. Since the amplitude of the scattered wave field in (1.58) varies inversely with distance from the scattering center, one could expect the free space Green's function to provide an accurate representation of the scattered field when the scattering object lies far from the boundaries of the background medium (*i.e.*, for weak reflections).

The utility of the Green's function (1.58) in solving (1.55) for an arbitrary object function $o(\vec{r})$ derives from the linearity of the Helmholtz equation. To see this, we observe that we can write the source term $u(\vec{r})o(\vec{r})$ of (1.55) as an integral over delta function impulses, where each impulse is positioned at a different coordinate $\vec{r}'$ in the acoustic medium:

$$u(\vec{r})o(\vec{r}) = \int_{V_0} o(\vec{r}')u(\vec{r}')\delta(\vec{r} - \vec{r}')d\vec{r}'. \tag{1.59}$$

Strictly speaking, the integration in (1.59) is performed over all three-dimensional space, but since the object function is nonzero only within the scattering object, (1.59) is also equal to the integral over just

the physical extent V_0 of the scattering object. Each impulse $\delta(\vec{r}-\vec{r}')$ in the preceding expression is weighted by the product of the total acoustic field $u(\vec{r}')=u_0(\vec{r}')+u_s(\vec{r}')$ and the object function $o(\vec{r}')$ present at the location $\vec{r}'$ of the impulse. This makes sense intuitively, since both $u(\vec{r}')$ and $o(\vec{r}')$ are related to the overall scattering power of the impulse at $\vec{r}'$. For example, if $o(\vec{r}')=0$, we are in the background medium where scattering of the acoustic wave field does not occur. On the other hand, in regions where $u(\vec{r}')=0,$ there is no a coustic field present to undergo scattering, so the scattering power of the impulses present in these regions is zero. We note that since $o(\vec{r}')$ is nonzero only for points lying within the physical dimensions of the scattering object, equation (1.59) constitutes a representation of the scattering source distribution as an array of point scatterers.

The Green's function (1.58) represents the solution for the scattered field $u_s(\vec{r})$ due to an object function $o(\vec{r})$ consisting of a single delta function impulse at $\vec{r}'$. Because the Helmholtz equation is linear, we can solve (1.55) by decomposing the source term $u(\vec{r})o(\vec{r})$ into an array of weighted impulses as in (1.59), solving (1.55) for each of these weighted impulses, and adding these individual solutions together to obtain the total solution to (1.55) for an arbitrary object function $o(\vec{r})$. In other words, since the scattered field due to the weighted impulse $o(\vec{r}')u(\vec{r}')\delta(\vec{r}-\vec{r}')$ at $\vec{r}'$ is simply the scaled Green's function

$$o(\vec{r}')u(\vec{r}')g(\vec{r}-\vec{r}')=o(\vec{r}')u(\vec{r}')\frac{e^{jk_0|\vec{r}-\vec{r}'|}}{4\pi|\vec{r}-\vec{r}'|}, \tag{1.60}$$

we find that the total scattered field at $\vec{r}$ due to the array of weighted impulses given by (1.59) is simply the superposition

$$u_s(\vec{r})=\int_{V_0} o(\vec{r}')u(\vec{r}')g(\vec{r}-\vec{r}')d\vec{r}'. \tag{1.61}$$

Equation (1.61) represents the solution to the inhomogeneous Helmholtz equation (1.55) for the scattered field due to an arbitrary object function $o(\vec{r})$. We recognize this expression as a three-dimensional convolution of the source function $u(\vec{r})o(\vec{r})$ with the Green's function $g(\vec{r}|\vec{r}')$. Equation (1.61) physically represents the total scattered pressure field at position $\vec{r}$ obtained through superposition of the separate scattered fields due to all of the individual point sources composing the scattering source distribution. It should be remembered that the acoustic field appearing in the integrand of (1.61) is the total field $u(\vec{r}') = u_0(\vec{r}') + u_s(\vec{r}')$. This makes sense physically; the amplitude of the field scattered by a single point source comprising the object depends on the total acoustic field incident on that particular point source. The field incident on a given point source in the object consists of a contribution from the incident field $u_0(\vec{r}')$ output by the transducer and a scattered field contribution $u_s(\vec{r}')$ due to the fields scattered by the other point sources in the object.

Equation (1.61) for $u_s(\vec{r})$ is actually an implicit solution to the inhomogeneous Helmholtz equation, since the integrand itself depends on the scattered field solution $u_s(\vec{r})$:

$$u_s(\vec{r}) = \int_{V_0} o(\vec{r}')\left[u_0(\vec{r}') + u_s(\vec{r}')\right] g(\vec{r} - \vec{r}')d\vec{r}'. \tag{1.62}$$

In the presence of weak scattering, the real and imaginary parts of the incident field amplitude $u_0(\vec{r}')$ are much larger than the corresponding parts of the scattered field amplitude $u_s(\vec{r}')$ for all $\vec{r}'$. This allows us to neglect the scattered field component of the total field in (1.62) to obtain an explicit solution for $u_s(\vec{r})$ in terms of the complex object function, the incident acoustic field (*i.e.*, the field calculated in (1.51)), and the Green's function (1.58):

$$u_s(\vec{r}) \cong u_B(\vec{r}) = \int_{V_0} o(\vec{r}')u_0(\vec{r}')g(\vec{r} - \vec{r}')d\vec{r}'. \tag{1.63}$$

Equation (1.63) expresses the so-called first-order Born approximation for the scattered field component of the total acoustic field. The Born approximation is iterative in nature, as substitution of (1.63) for $u_s(\vec{r})$ back into (1.62) can improve the accuracy of the initial estimate for $u_s(\vec{r})$. This procedure would yield the second-order Born approximation for the scattered field, which itself could be substituted back into (1.62) for $u_s(\vec{r})$ to obtain yet another improvement in the estimate of the scattered field. In principle, this process can be repeated an arbitrary number of times to obtain the i^{th}-order Born estimate for the scattered field amplitude $u_s(\vec{r})$. The i^{th}-order Born approximation for the scattered field is given by

$$u_B^{(i)}(\vec{r}) = \int_{V_0} o(\vec{r}')\left(u_0(\vec{r}') + u_B^{(i-1)}(\vec{r}')\right)g(\vec{r}-\vec{r}')d\vec{r}', \qquad (1.64)$$

where $u_B^{(0)}(\vec{r}') = 0$. Equation (1.64) is identical to (1.62), with the exception that $u_s(\vec{r}')$ has been replaced by the estimate $u_B^{(i-1)}(\vec{r}')$. For our purposes, particularly those related to tomographic reconstruction, we will find the first-order Born field as given by (1.63) to be the most useful of the iterative Born approximations.

Before considering how the first-order Born approximation can be used for tomographic reconstruction, it is instructive to examine (1.63) more closely to understand the fundamental physical assumptions underlying the Born theory. Based on our previous discussion concerning the decomposition of a continuous scattering distribution into an array of point scattering centers, we see that (1.63) suggests that the field incident on each point scatterer in the object is simply $u_0(\vec{r}')$, the incident acoustic field output by the transducer. Thus, (1.63) implies that the incident field output by the transducer remains essentially unchanged as it passes through the scattering object. For a homogeneous cylinder of radius *a* having an acoustic refractive index deviation $n_\delta(\vec{r}) = n_\delta$ relative to the refractive

index of the background medium, it is possible to show that the Born assumption of a negligible perturbation of the incident transducer field is satisfied under the condition

$$an_{\delta} < \frac{\lambda}{4}, \tag{1.65}$$

where λ denotes the wavelength of the acoustic wave field in the background medium. Therefore, a distinctive feature of the first-order Born approximation is that the conditions for its validity depend not only on the refractive index of the imaged object but also on its size.

Because of its conduciveness to tomographic reconstruction, from this point forward, we will consider only the first-order Born approximation for the scattered field,

$$u_s(\vec{r}) \cong u_B(\vec{r}) = \int_{V_0} o(\vec{r}')u_0(\vec{r}')g(\vec{r}-\vec{r}')d\vec{r}', \tag{1.66}$$

where the incident field $u_0(\vec{r}')$ is the output of the acoustic transducer that we calculated in (1.51), namely

$$u_0(x',y',z') = -j\rho_0 v_0 f\left[\frac{e^{jk_0 r'}}{r'} ** \text{rect}\left(\frac{x'}{a}\right)\text{rect}\left(\frac{y'}{a}\right)\right]. \tag{1.67}$$

In a single transmission image of an object, ultimately what is measured in the detector plane is the intensity of the total acoustic field $u(\vec{r})$, which includes components due to both the transducer output as well as scattering from the object being imaged:

$$u(\vec{r}) = u_0(\vec{r}) + u_s(\vec{r}). \tag{1.68}$$

By adding (1.66) and (1.67), we have a predictive model for the spatial variation in acoustic intensity $I(\vec{r})$ that would be measured in the detector plane for an arbitrary object being imaged:

$$I(\vec{r}) = \left|\int_{V_0} o(\vec{r}')u_0(\vec{r}')g(\vec{r}-\vec{r}')d\vec{r}' - j\rho_0 v_0 f\left[\frac{e^{jk_0 r}}{r} ** \text{rect}\left(\frac{x}{a}\right)\text{rect}\left(\frac{y}{a}\right)\right]\right|^2. \tag{1.69}$$

V. Algorithms for Ultrasound Tomographic Reconstruction

The goal of any tomography experiment involving the imaging of a three-dimensional object is accurate volumetric reconstruction of the object from a series of two-dimensional planar projections. In ultrasound diffraction tomography, since spatial variations in the acoustic refractive index are responsible for wave field scattering, what we are actually reconstructing is a three-dimensional mapping of the real and imaginary parts of the acoustic refractive index of the object immersed in the background medium.

Fundamental to diffraction tomography is the Fourier Diffraction Theorem (FDT), which is analogous to the Central Slice Theorem of x-ray computed tomography. In fact, by use of fractional Fourier transforms, it can be shown that both theorems are equivalent in the short-wavelength limit. The FDT relates the two-dimensional Fourier transform of the scattered component $u_s(\vec{r})$ of the total acoustic field measured in the detector plane to the three-dimensional Fourier transform of the object function itself. The FDT is extremely powerful and enables the Fourier space of the object function to be built up from a series of two-dimensional planar projections. Fourier inversion of this result provides an estimate of the object function directly. It should be realized that the FDT is valid only in the presence of weak scattering by inhomogeneities in the imaged object.

The measurement geometry of ultrasound diffraction tomography consists of an acoustic source and a planar detector that are diametrically opposed and positioned on oppos ite sides of the inhomogeneous object being imaged. For ultrasound illumination of the object $o(\vec{r})$ using a single plane wave, the FDT states that the two-dimensional Fourier transform of the forward scattered field $u_s(\vec{r})$ measured over the detector plane is equal to a hemispherical surface in the three-dimensional Fourier space of the object function $o(\vec{r})$. This surface passes through the origin of the object Fourier space and is oriented opposite the propagation direction of the probing plane wave field. Moreover, the

radius of the hemispherical surface is determined by the wave vector magnitude (*i.e.*, the wavelength) in the background medium of the ultrasound energy used to illuminate the object. By rotating the detector and source assembly around the object and imaging at different angular positions, the Fourier space of the object can be built up using the hemispherical surfaces provided by the distinct source-detector positions. In practice, a number of discrete angular positions of the source and detector are employed, and appropriate interpolation techniques are then used to estimate the values of the Fourier transform of the object function where measurement data is not available. The interpolated Fourier space representation of the object is then inverted to obtain an estimate of the object function $o(\vec{r})$.

For an arbitrary source of acoustic waves, the FDT as outlined in the preceding paragraph is not directly applicable, since the incident pressure field may not be a simple plane wave. In particular, the incident acoustic wave field relevant to our ultrasound system is given by the convolution of (1.51). We recall, however, that the expression we derived in (1.51) for the incident field was based on an angular spectrum decomposition method involving a superposition of plane wave solutions to the homogeneous Helmholtz equation. Thus, it is reasonable to expect due to the linearity of the Helmholtz equation that alternative methods based on the FDT exist for filling the Fourier space of an object using arbitrary wave fields. Such algorithms have previously been developed, and we present one of these methods in this section. The advantage of this procedure is that it requires only two angular orientations of the object separated by 90^{o}. It is based on acquiring measurements of the scattered field throughout the detector plane as the position of the acoustic source is varied in the transducer plane. Obtaining diffracted projections of the object in this manner has the added benefit of more closely resembling the B-mode scanning procedure of conventional pulse-echo ultrasound imaging, a procedure with which most everyone is familiar.

The development of the aforementioned reconstruction method involves writing the volume integral (1.63) representing the first-order Born approximation in a way that relates the Fourier

transform of the object function to the Fourier transform of the scattered field. This procedure can be performed by making use of the angular spectrum method outlined in section II. In particular, we showed previously that for an ultrasound transducer centered at the origin of coordinates in the transducer plane, the angular spectrum decomposition of the incident acoustic field $u_0(\vec{r})$ in any plane of constant *z* is given by

$$u_0(\vec{r}) = \frac{1}{4\pi^2}\int_{-\infty}^{\infty}\int_{-\infty}^{\infty}\alpha(k_x, k_y : z=0)e^{j(k_x x + k_y y + k_z z)}dk_x dk_y, \tag{1.70}$$

where all variables are defined as they were in section II and we recall that $k_z = \sqrt{k_0^2 - k_x^2 - k_y^2}$. If we consider a translation of the transducer surface from the coordinate origin of the transducer plane to the point (x_t, y_t) in that plane, then it follows from (1.70) that the angular spectrum decomposition of the transducer field $u_0(\vec{r} : x_t, y_t)$ is given by

$$u_0(\vec{r} : x_t, y_t) = \frac{1}{4\pi^2}\int_{-\infty}^{\infty}\int_{-\infty}^{\infty}\alpha(k_x, k_y : z=0)e^{j(k_x(x-x_t) + k_y(y-y_t) + k_z z)}dk_x dk_y. \tag{1.71}$$

Equation (1.71) represents a simple shift of the entire incident field expressed in (1.70) by x_t in the *x*-direction and y_t in the *y*-direction. This is just what we expect, since the only physical difference between the situations described by (1.70) and (1.71) is a relative shift (x_t, y_t) of the transducer position in the source plane.

Considering now the free space Green's function given by (1.58), we observed earlier that a spherical wave centered at the origin and characterized by a w ave vector of magnitude k_0 has the angular spectrum decomposition shown in (1.50), namely

$$\frac{1}{j2\pi}\frac{e^{jk_0 r}}{r} = \frac{1}{4\pi^2}\int_{-\infty}^{\infty}\int_{-\infty}^{\infty}\frac{e^{j\left(k_x x + k_y y + z\sqrt{k_0^2 - k_x^2 - k_y^2}\right)}}{\sqrt{k_0^2 - k_x^2 - k_y^2}}dk_x dk_y, \tag{1.72}$$

where $z \geq 0$. From (1.72), it follows that the angular spectrum decomposition of the Green's function (1.58) is given by

$$\frac{1}{4\pi}\frac{e^{jk_0|\vec{r}-\vec{r}'|}}{|\vec{r}-\vec{r}'|} = \frac{j}{2}\left[\frac{1}{4\pi^2}\int_{-\infty}^{\infty}\int_{-\infty}^{\infty}\frac{e^{j\left(\alpha(x-x')+\beta(y-y')+(z-z')\sqrt{k_0^2-\alpha^2-\beta^2}\right)}}{\sqrt{k_0^2-\alpha^2-\beta^2}}d\alpha d\beta\right], \qquad (1.73)$$

where $\vec{k}_0 = (\alpha, \beta, \sqrt{k_0^2-\alpha^2-\beta^2})$.

If we insert the decompositions (1.71) and (1.73) into the first-order Born approximation (1.63), we obtain an approximate expression for the scattered field when the transducer is centered at (x_t, y_t) in the transducer plane:

$$u_s(\vec{r}:x_t,y_t) \cong \frac{j}{2(2\pi)^4}\int_{V_0} o(\vec{r}')\left[\int_{-\infty}^{\infty}\int_{-\infty}^{\infty}\frac{e^{j\left(\alpha(x-x')+\beta(y-y')+(z-z')\sqrt{k_0^2-\alpha^2-\beta^2}\right)}}{\sqrt{k_0^2-\alpha^2-\beta^2}}d\alpha d\beta\right]\times \qquad (1.74)$$

$$\left[\int_{-\infty}^{\infty}\int_{-\infty}^{\infty}\alpha(k_x,k_y:z'=0)e^{j(k_x(x'-x_t)+k_y(y'-y_t)+k_z z')}dk_x dk_y,\right]d\vec{r}'.$$

For a p lanar detector lying in the plane $z = D$, the scattered field amplitude at the position $\vec{r} = (x_r, y_r, D)$ in the detector plane is therefore given by

$$u_s(\vec{r}:x_t,y_t) \cong \frac{j}{2(2\pi)^4}\int_{V_0} o(\vec{r}')\left[\int_{-\infty}^{\infty}\int_{-\infty}^{\infty}\frac{e^{j\left(\alpha(x_r-x')+\beta(y_r-y')+(D-z')\sqrt{k_0^2-\alpha^2-\beta^2}\right)}}{\sqrt{k_0^2-\alpha^2-\beta^2}}d\alpha d\beta\right]\times \qquad (1.75)$$

$$\left[\int_{-\infty}^{\infty}\int_{-\infty}^{\infty}\alpha(k_x,k_y:z'=0)e^{j(k_x(x'-x_t)+k_y(y'-y_t)+k_z z')}dk_x dk_y,\right]d\vec{r}'.$$

Letting $x_t \to -x_t$ and $y_t \to -y_t$ in (1.75) gives

$$u_s(\vec{r}:-x_t,-y_t) \cong \frac{j}{2(2\pi)^4}\int_{V_0} o(\vec{r}')\left[\int_{-\infty}^{\infty}\int_{-\infty}^{\infty}\frac{e^{j\left(\alpha(x_r-x')+\beta(y_r-y')+(D-z')\sqrt{k_0^2-\alpha^2-\beta^2}\right)}}{\sqrt{k_0^2-\alpha^2-\beta^2}}d\alpha d\beta\right]\times \qquad (1.76)$$

$$\left[\int_{-\infty-\infty}^{\infty}\int^{\infty}\alpha(k_x,k_y:z'=0)e^{j(k_x(x'+x_t)+k_y(y'+y_t)+k_z z')}dk_x dk_y,\right]d\vec{r}'.$$

Taking the two-dimensional Fourier transform of both sides of (1.76) with respect to the spatial coordinates (x_t, y_t) of the transducer position, and then taking the two-dimensional Fourier transform of both sides of the resulting equation with respect to the spatial coordinates (x_r, y_r) of the field point in the detector plane gives

$$U_s(\alpha,\beta;k_x,k_y)=\frac{je^{jD\sqrt{k_0^2-\alpha^2-\beta^2}}}{2\sqrt{k_0^2-\alpha^2-\beta^2}}\alpha(k_x,k_y:z'=0)\times \tag{1.76}$$

$$\int_{V_0} o(\vec{r}')e^{-j(x'(\alpha-k_x)+y'(\beta-k_y)+z'(\sqrt{k_0^2-\alpha^2-\beta^2}-\sqrt{k_0^2-k_x^2-k_y^2}))}d\vec{r}',$$

where $U_s(\alpha,\beta;k_x,k_y)$ of (1.76) is related to the scattered field amplitude $u_s(\vec{r}:-x_t,-y_t)$ in the plane $z = D$ according to

$$U_s(\alpha,\beta;k_x,k_y)=\int_{-\infty-\infty}^{\infty}\int^{\infty}\left[\int_{-\infty-\infty}^{\infty}\int^{\infty}u_s(x_r,y_r,D:-x_t,-y_t)e^{-j(k_x x_t+k_y y_t)}dx_t dy_t\right]\times \tag{1.77}$$

$$e^{-j(\alpha x_r+\beta y_r)}dx_r dy_r.$$

Recognizing the integral in (1.76) as the three-dimensional Fourier transform of the object function $o(\vec{r}')$ evaluated at $(\alpha-k_x,\beta-k_y,\gamma-k_z)$ enables us to write (1.76) as

$$U_s(\alpha,\beta;k_x,k_y)=\frac{je^{jD\gamma}}{2\gamma}\alpha(k_x,k_y:z'=0)O(\alpha-k_x,\beta-k_y,\gamma-k_z), \tag{1.78}$$

where $\gamma=\sqrt{k_0^2-\alpha^2-\beta^2}$ and $k_z=\sqrt{k_0^2-k_x^2-k_y^2}$. It can be shown using (1.78) that the scattered field data obtained for a single projection of the object yields coverage in the frequency domain of the object function defined by two spheres. A single projection view in this imaging procedure corresponds to a single orientation of the object relative to the source plane but multiple transducer positions in the

source plane. For a single projection view, the scattered field is collected in the detector plane as a function of the transducer position in the source plane. By rotating the object 90^{o} and performing the same scanning procedure of the transducer in the source plane, it is possible to generate the complementary spheres in the frequency domain of the object function and thus fill in the Fourier space of the object.